Final Report for AOARD-07-4052
Enhancement of POD for structural health monitoring of bonded repaired structures

Date 4 Jan 2010

Principal Investigators:

Names	W.K. Chiu	F.K. Chang
Email address	w.chiu@eng.monash.edu.au	fkchang@stanford.edu
Institution	Monash University, Australia	Stanford University, USA
Mailing Address	P.O. Box 31 Monash University Victoria Australia 3800	Dept of Astronautics and Aeronautics 496 Lomita Mall, Stanford University Stanford, California 94305 USA
Phone	+ 61 3 9905 5595	+1 650 723 3466
Fax	+ 61 3 9905 1825	+1 650 725 3377

Period of Performance: Sep 2007 – Sep 2009

Abstract: This paper discusses the scattering of stress waves by defects in representative aircraft structures with multi-layered construction and geometry variation. The approaches for determining and enhancing the probability of detection of non-surface penetrating defects in such structures as well as minimising the contributions of multi-layered construction and geometry variation to false indications are presented. The results demonstrate the importance of selecting the appropriate frequency and location of the sensor in monitoring subsurface defects on these structures. The findings suggested that a computer solution of the problem may be required to determine the optimal combination of frequency and sensor location. This study suggests the possibility of incorporating structural health monitoring into the design of future structures which will constitute a significant leap in the current knowledge base of structural health monitoring.

1.   Introduction: The potential of stress wave based structural health monitoring methodologies has been widely explored in recent years. The main driver behind this exploration is the high sensitivies of stress waves to small, surface and sub-surface defects in metallic [1] and composite structures [2]. Moreover, the ability of stress waves to travel over long distances within these structures has greatly increased the potential in detecting defects at locations that are difficult to access. However, the propagation of stress waves in multi-layered structures can be scattered by geometry variations, material inhomogeneities and/or structural defects. It is therefore the aim of this paper to build on this knowledge specifically for the benefit of in-situ structural health monitoring (ISHM).

ISHM based on propagating stress waves relies on a network of actuating and sensing piezoelectric elements, which are bonded onto the structure. The issues of "false negatives" and "false positives" are major impediments to the practical application of ISHM. In this paper the terms "false negatives" and "false positives" are identified collectively as examples of information infidelity (INF). While the issue of INF is relevant to all modes of ISHM, this study addresses only stress-wave based methodologies. Researchers have reported on the effects of the governing physics, sensor durability, sensor bond durability and environmental effects on this stress wave based methodology. For example, the effects of operational environment (e.g. temperature fluctuations) were addressed by Rajic et al [3]. Hoon et al [4] have described the impact of sensor bond integrity and sensor durability on INF. Whilst all factors affecting stress-wave based methodologies outlined above are germane to INF, the physics governing the interaction of the measurand to the existence of defects and structural variations is of paramount importance.

Callinan et al [6] reported on the development of fatigue cracks on the F-111 underwing skin. This report also documented the use of a boron/epoxy doubler to repair the damage region. The fatigue crack was reported to have developed as a sub-surface defect on the inside of the wing and propagated outwards. Since it is not feasible to inspect the inside of the wing skin, nor to apply sensors on the

Report Documentation Page		*Form Approved* *OMB No. 0704-0188*

1. REPORT DATE **04 JAN 2010**	2. REPORT TYPE **FInal**	3. DATES COVERED **01-09-2007 to 31-08-2009**

4. TITLE AND SUBTITLE **Enhancement of POD for structural health monitoring of bonded repaired structures**	5a. CONTRACT NUMBER **FA48690714052**
	5b. GRANT NUMBER
	5c. PROGRAM ELEMENT NUMBER
6. AUTHOR(S) **Wing Kong Chiu**	5d. PROJECT NUMBER
	5e. TASK NUMBER
	5f. WORK UNIT NUMBER
7. PERFORMING ORGANIZATION NAME(S) AND ADDRESS(ES) **Monash University,P.O. Box 31, Monash University, Wellington Road,Clayton, Victoria 3800,Australia,AU,3800**	8. PERFORMING ORGANIZATION REPORT NUMBER **N/A**
9. SPONSORING/MONITORING AGENCY NAME(S) AND ADDRESS(ES) **AOARD, UNIT 45002, APO, AP, 96337-5002**	10. SPONSOR/MONITOR'S ACRONYM(S) **AOARD**
	11. SPONSOR/MONITOR'S REPORT NUMBER(S) **AOARD-074052**

12. DISTRIBUTION/AVAILABILITY STATEMENT
Approved for public release; distribution unlimited

13. SUPPLEMENTARY NOTES

14. ABSTRACT

This paper discusses the scattering of stress waves by defects in representative aircraft structures with multi-layered construction and geometry variation. The approaches for determining and enhancing the probability of detection of non-surface penetrating defects in such structures as well as minimizing the contributions of multi-layered construction and geometry variation to false indications are presented. The results demonstrate the importance of selecting the appropriate frequency and location of the sensor in monitoring subsurface defects on these structures. The findings suggested that a computer solution of the problem may be required to determine the optimal combination of frequency and sensor location. This study suggests the possibility of incorporating structural health monitoring into the design of future structures which will constitute a significant leap in the current knowledge base of structural health monitoring.

15. SUBJECT TERMS
Aging Aircraft, Aircraft Structures

16. SECURITY CLASSIFICATION OF:			17. LIMITATION OF ABSTRACT	18. NUMBER OF PAGES	19a. NAME OF RESPONSIBLE PERSON
a. REPORT **unclassified**	b. ABSTRACT **unclassified**	c. THIS PAGE **unclassified**	**Same as Report (SAR)**	**30**	

inside surface, the use of in situ acoustic transducers installed on the outer wing surface was considered a viable means of inspection.   Lamb waves produced by the transducers would provide the interrogating field. However, Lamb waves are scattered not only by defects, but also by geometrical features like integral stiffeners, which form part of the F-111 wing structure. The work discussed in this paper shall address the issues relating to the detection of this type of sub-surface crack in an aluminium structure. This paper shall also report on the ability to use a stress-wave methodology for the monitoring of fatigue crack development when the structure is repaired using a bonded boron/epoxy doubler.

In this paper, the scattering of stress waves by defects or service-induced damage in representative aircraft structures with multi-layered construction and geometry variation is characterised. This knowledge shall be used in the development of a robust structural health monitoring scheme. In addition, the approaches for determining and enhancing the probability of detection (POD) [5] of non-surface penetrating defects in such structures, as well as minimising the contributions of multi-layered construction and geometry variation to INF are demonstrated. In this respect, the work reported on in this paper can lead to the removal of this impediment which will constitute a significant leap in the current knowledge base of structural health monitoring.

This study is organised as follows: The models used for the investigation as well as the process of determining INF and POD are described in Section 2. Section 3 reports the results of a series of computational investigations to determine the effects of the presence of sub-surface defects on the propagation of stress waves in a flat plate and in a structure with geometry variations. The results highlighted the importance in the appropriate characterisation of the time (i.e. frequency) scale and length scale of the problem prior to the establishment of an appropriate ISHM strategy. This can help in minimising or elimination of the occurrence of false indications.

2.   Experiment:

2.1   Whilst focusing on the problems described by Callinan et al [6] a series of investigations using finite element analyses have been conducted to determine the effects of;
   1) the presence of the sub-surface defects on the propagation of stress waves,
   2) the presence of geometry variations (including a   sub-surface defect) on the propagation of stress waves, and
   3) the presence of geometry variations (including a sub-surface defect) and repair patch on the propagation of stress waves

To achieve these aims, a series of models were considered. Firstly, a model of an aluminium flat plate (Model #1) was considered. A series of sub-surface defects were introduced in the model. The primary purpose of this model is for demonstrating the interaction of sub-surface defects with the impinging stress wave. In this second model, an aluminium plate with geometry variations was considered (Model #2). The series of sub-surface defects included in the first model were also induced in this model. These analyses will highlight the interaction of the impinging stress wave with the geometry variations and the sub-surface defect. In the third model (Model #3), a boron/epoxy doubler was introduced to Model #2 to simulate a bonded structural repair.

A schematic of the cross-sectional view of the models used for these three cases are shown in Figure 1. Model #1 is a flat aluminium plate of dimensions 3.6mm x 100.0mm x 140.0mm and the 3.6mm x 140.0mm face is shown in Figure 1. The isometric view of the model with geometry variation (denoted as Model #2 and Model #3), is shown in Figure 2. This represents the lower wing skin of the F-111. Figure 3 shows the finite element model of the structure shown in Figure 2 and the region where the data are extracted for analyses. The mechanical properties of the materials used in the finite element analyses are reported in Table 1.

To simulate the development of a sub-surface defect in the underwing skin, notches of three different sizes are used, namely 33%, 67%, 100% (representing penetration of the skin) were used. The profile and dimensions of these notches are shown in Figure 4 and Table 2, respectively. The excitation used is shown in Figure 5. This pulse has a wide frequency bandwidth. The results presented in this paper shall be analysed within a bandwidth of 100 kHz-600 kHz. Within this frequency bandwidth, it is

expected that a number of Lamb wave modes are excited. The propagation of the Lamb wave modes shall be analysed from the displacement field calculated resulting from the pulse input.

2.2 Probability of detection

Probability of detection (POD) is often used in non-destructive inspection procedures. The POD of an NDI methodology to detect a given defect size is dependent on several parameters including device placement, operator, surface conditions and couplant [9]. In the case of ISHM, the sensor placements and surface conditions are pre-determined and do not change with time. There is also no issue with change in operator. In this respect, the term "probability of detection" (POD) used for ISHM should be different from that of traditional NDI and shall first be defined. In the monitoring methodology proposed in this paper, as in many others, the change in the received signal with respect to the "undamaged" case is used as an indication of the development of a defect. In this respect, we firstly assume that there is a probability of 1 when, for a given defect size, the received signal is reduced by 90% of its initial "undamaged" value. A probability of 0 is assumed when the change in the received signal is reduced by 10% or less. For the purpose of this investigation, in order to demonstrate the concept of POD, we shall assume a linear variation in the probability in the intermediate levels of received signal reduction. Using this definition of POD, it is envisaged that the spatial variation in the POD calculated can be used as a guide for optimal sensor location. In this respect, the optimal sensor location shall reside in regions of maximal POD.

In this following analysis, the changes in the amplitude of the stress wave resulting due to the presence of a defect shall be documented. The calculated amplitude shall be deemed as the mean value and it shall be assumed that the distribution of the magnitudes of this measured response can be described by the Gaussian probability density function (PDF) [7],

$$PDF = \frac{1}{\sigma\sqrt{2\pi}} e^{-\left[\frac{(A-m)^2}{2\sigma^2}\right]}$$ Eq. (1)

where σ is the standard deviation and m is the mean. A is magnitude of the x-axis of the PDF. Samples of the Gaussian PDF are plotted in Figure 6, and PFI is defined as the probability of a false indication [8]. From Figure 6, the relationships among POD, PDF and PFI are described in Eqs. (2) and (3). In conventional ultrasonic testings, the standard deviation (SD) values are also dependent on parameters such as the probe couplant, operator, and surface conditions of specimen [9]. However, this is not the case in the SHM context where the transducer is fixed, as the errors due to transducer couplant and the positioning of transducers are eliminated.

A literature search on the parameters and the corresponding effects that the SD values are dependent on reveals that very limited work has been conducted in this area. This paper does not aim not to study the effects of the above mentioned SD related variables but to demonstrate the spatial and temporal effects on the POD of a given defect size occurring in the test specimen. In these analyses, the SD of 0.07 was used and is based on those suggested by Harding et al [7] (i.e. for a notch created with electrical discharge machining).

$$POD = \int_T^\infty PDF_{damage} dA - \int_T^\infty PDF_{undamage} dA$$ Eq. (2)

$$PFI = \int_T^\infty PDF_{undamage} dA$$ Eq. (3)

where T is the threshold, or the intersection point in Figure 6.
The process of determining the POD is as follows:
  i.   Normalise the response magnitudes for the damaged case with respect to those measured for the undamaged case.
  ii. Eliminate ratios that exceed a value of 1, i.e. cases where the response magnitude increases with respect to size of defect.

iii.   Adjust the ratios so that the mean of the undamaged case is 0, i.e. $m = 0$.
iv.   Determine the intersection.
v.   Calculate the POD using Eq. (2).

In process stage (ii), the ratios that exceed a value of 1 are eliminated to reduce the confusion in calculating POD. The increase in the amplitude of the stress wave can occur because of the scattering of the stress wave. This increase has been shown to be in the order of 10% of the original energy, whilst observable in experiments shall be deemed to be at the limits of experimental variations and uncertainties in this paper. At this level of change it shall be considered difficult to differentiate whether or not an increase in displacement field is caused by a small sub-surface defect. Therefore, we shall classify this as a "null" result. In this paper we shall focus on the fact that energy transferred downstream of the model will be generally decrease as the size of sub-surface defect is increased.

3.   Results and Discussion:
3.1 Flat plate with sub-surface defect (Model #1)
Figure 7 shows the dispersion characteristics of the flat plate model. The solid lines in this plot refer to Lamb wave modes identified from the displacement field in the plate. This set of results show that several Lamb wave modes were excited. In order to investigate the temporal and spatial characteristics of the wave on the model, the results were plotted as a function of frequency and distance along the centre line of the model. Figure 8 shows the magnitude of the displacement field as a function of frequency and distance. These data were extracted from the model along the line shown in Figure 3. Figure 8b shows the region of the model downstream of the location where the defect is to be introduced. It is evident from Figure 8a that there is a decrease in the intensity of the stress wave as a function of distance from the source. This is expected in wave propagation.

Figure 9 shows the case where a sub-surface defect was introduced at the location shown in Figures 2 and 3. In this case, the depth of the sub-surface defect is 33% of the plate thickness (see Figure 4). Interference of the incident and reflected stress wave at the defect location is evident in Figure 9. The values of POD described above were calculated using standard deviations of 0.07 is presented in Figure 10. It is evident from Figure 10 that the POD is a function of both sensor location and acoustic drive frequency. The spatial dependence can only arise due to the scattering of the stress waves by the sub-surface defect.

Figure 11 shows the results obtained for a defect depth of 67% of the plate thickness. It is noted in Figure 11 that the region of interference of the incident wave and that reflected wave from the sub-surface defect is more pronounced than that found in Figure 9 due to the larger defect size. This confirms the earlier evident of the existence of this interference region. The POD calculated is shown in Figure 12. The results are similar to that shown in Figure 10. With a larger defect size, the POD appears to have increased. However, the ability to monitor the development of this defect is highly dependent on the location of the sensor.

Figure 13 shows the results obtained with a sub-surface defect that has penetrated the surface. It is shown that the magnitude of the stress waves downstream of the defect is limited. The POD calculated is shown in Figure 14. There is one fascinating feature about the results shown in Figure 14. Although the defect has now penetrated the surface of the structure, the POD is still very much dependent on the frequency, and the spatial characteristics of the distribution are still evident. This is explained by the fact that even though the defect has penetrated the surface, the dimension of the defect on the underside is considerably larger (see Figures 3 and 4). The varying geometry of the defect in the through-thickness direction will scatter the incident stress wave. In addition, as the crack was straight-sided and not curved, the edges will scatter the field and so produce zones of high and low intensity downstream.

3.2 Plate with geometry variation with sub-surface defect (Model #2)
As shown in Figure 1, the difference between the model considered here and that described in Section 3.1 is the presence of geometry variations. Figure 15 shows the temporal-spatial characteristics of the displacement field obtained from the model. Although the results were obtained from the model without any defect, regions of interference of the incident and reflecting stress wave is present (compare with Figure 8b). This is attributed to the geometry variation present because it is located in

its vicinity. It can also be noted that the interferences are more significant at higher frequency (comparing Figures 8a and 15). This further attests to the scattering of the incident stress wave by the geometry variation. In addition, these results suggest that relying on reflection from the defect as an indication of damage with this geometry variation can be difficult due to the need to separate the reflection due to geometry variation and that due to the presence of sub-surface defect. This is because of the relative insignificance of the effects from sub-surface defect with respect to those of geometry variation.

Figure 16 shows the results obtained with a sub-surface defect that is 33% of the plate thickness. The POD calculated is shown in Figure 17. These results suggested that the choice of frequency is crucial if the defect is to be monitored without any false indication. The optimal frequency for detection is different to that for the flat plate. As in the previous case, the spatial dependence is also significant. This signifies that the length and time-scale of the ISHM methodology is geometry dependent, that is, problem dependent.

Figure 18 shows the results obtained with a sub-surface defect that is 67% of the plate thickness. The POD calculated is shown in Figure 19. This figure suggests that the choice of frequency has not changed from that in Figure 17. Figure 20 shows the results obtained with a defect that has penetrated the surface. The POD calculated is shown in Figure 21 and the choice of frequency has not altered.

3.3 Plate reinforced with boron/epoxy with geometry variation with sub-surface defect (Model #3) (on aluminium surface)

The model considered in Section 3.2 above is now reinforced with a boron/epoxy patch to simulate the repaired condition. In this section the results presented were obtained from data extracted on the aluminium surface beneath the patch, representing the case where sensors are embedded in the bondline of the patch. Figure 22 shows the temporal-spatial characteristics of the displacement wave field. Similar to the results shown in Figure 15, there exists a region where interference of the incident and reflecting stress wave is present. This result shows that the boron/epoxy patch does not alter the scattering caused by the geometry variations in the sample.

Figure 23 shows the results obtained with a sub-surface defect that is 33% of the plate thickness. The POD calculated is shown in Figure 24. The choice of frequency is similar to that described in Section 3.2. This suggests that the propagation characteristics of the stress wave are governed pre-dominantly by the aluminium parent structure. The spatial dependence observed earlier is still significant.

Figure 25 shows the results obtained with a sub-surface defect that is 67% of the plate thickness. The POD calculated is shown in Figure 26. The result here differs from the preceeding cases in that the optimal frequency for detection appears to change with defect size. As an example, the POD for the 33% penetration case at 300 kHz at location 0.045 m is drastically diminished (Figure 23) as compared to Figure 25. However, locating the sensing point at 0.055 m at this frequency improves the probability of detecting this defect. This implies that locating the sensing point at 0.045 m with a 300 kHz stress wave can result in a false negative. These results demonstrated that the choice of location not only affects the sensitivity and the POD, it can also give rise to false negatives. Based on this observation, the placement of sensors and the choice of frequency for ISHM are not arbitrary but problem-driven.

Figure 27 shows the results obtained with a defect that has penetrated the surface. The POD calculated is shown in Figure 28. This figure shows that at 300 kHz, the similar probability of detection is expected when locating the sensor at 0.045 m and 0.055 m.

3.4 Plate reinforced with boron/epoxy with geometry variation with sub-surface defect (Model #3) (on boron/epoxy surface)

In this section, the results are obtained from data extracted from the surface of the boron/epoxy patch to simulate the case where sensors are surface-mounted. Figure 29 shows the temporal-spatial characteristics of the displacement field calculated on the boron/epoxy patch. The results shown did not include stress wave interference regions obtained at the aluminium surface. This shows that the magnitude of the stress wave decreases, much the same as that for the flat aluminium plate.

The magnitude of the stress wave along the line shown in Figure 3 with sub-surface defects of 33%, 67% of the plate thickness, and a fully penetrating defect are shown in Figures 30, 32 and 34, respectively. These results does not reveal the reflection of the stress wave from the defects. This highlights the apparent futility in using the the reflection phenomena as a means of damage monitoring when placing sensors on the boron/epoxy surface. The respective POD downstream of the defect calculated with these models are shown in Figures 31, 33 and 35. The spatial dependence of the POD is evident. These results reinforce the earlier observation that the driving frequency and sensor location were equally critical in the case where measurements were taken on the repair patch surface.

4. Conclusions
The following conclusions were made from the findings described above.

(1) The frequency choice and the sensor location are of critical importance in monitoring subsurface defects on flat aluminium plates and on plates with geometry variations. In addition, these parameters are significant when monitoring defects on repaired structures with geometry variations.

(2) The choice of frequency and the optimal location of the sensor can only be established with a good understanding of the problem.

(3) An arbitrary location of the sensor can lead to false negatives. In this respect, a computer solution of the problem may be required to determine the optimal combination of frequency and sensor location.

(4) The importance of computational work has been demonstrated in this study. Overall, the study suggests the possibility of incorporating SHM into the design of future structures.

List of Publications:
W.K. Chiu, T.Tian (2008) Effects of structural geometry on health monitoring, New Challenges in Aerospace Technology & Maintenance Conference 2008, 15-16 Feb, Suntec City, Singapore.

Y.H. Teo, W.K. Chiu, N. Rajic, F.K. Chang (2008) The influence of Lamb wave modes on the detectability of sub-surface cracks, Materials Forum, Vol 33, pp 472-478

C. Doherty, W.H. Ong, W.K. Chiu (2008) The effects of geometry variation on fatigue crack monitoring using propagating Lamb waves, Materials Forum, Vol 33, pp 465-471

W.K. Chiu, T. Tian, F.K. Chang (2008) The effects of structural variations on the health monitoring of composite structures, Composite Structures, Vol 87, pp 121-140

Teo, Y.H, W.K. Chiu, F.K. Chang, N. Rajic (2008) Optimal placement of sensors for sub-surface fatigue crack monitoring, Theoretical and Applied Fracture Mechanics, Vol 52, pp 40 - 49

References

[1] W.J. Staszewski, B. C. Lee, L. Mallet and F. Scarpa, Structural health monitoring using scanning laser vibrometry: I. Lamb wave sensing, Smart. Mater. Struct. 13 (2004) 251-260

[2] D.E. Chimenti, and R. W. Martin, Nondestructive evaluation of composites laminates by leaky Lamb waves, Ultrasonics 29 (1991) 13-21

[3] N. Rajic, S. C. Galea and W.K. Chiu, Autonomous detection of crack initiation using surface-mounted piezotransducers, Smart Mater. Struct. 11 (2002) 107-114

[4] T.H. Hoon, D.W. Cheam and W.K. Chiu, edited by F.K. Chang, Mechanical Degradation of the Piezoelectric Elements, in Structural Health Monitoring 2005: Advancements And Challenges for Implementation (DEStech Publications Inc, 2005)

[5] A.P. Berens and P. W. Hovey, Statistical methods for estimating crack detection probabilities (ASTM, 1983)

[6] R.J. Callinan, S. Sanderson and D. Kelly, Finite element analysis of an F-111 lower wing skin fatigue crack repair (DSTO Scientific Publications, 1997)

[7] C. Harding, G. Hugo and S. Bowles, Model-assisted probability of detection validation of automated ultrasonic scanning for crack detection at fastener holes, 10th Joint Conference on Aging Aircraft. Palm Springs, CA, USA (2007)

[8] J.A. Ogilvy, Model for predicting ultrasonic pulse-echo probability of detection, NDT Int. 26 (1993) 19-29

[9] C.A. Hogarth and J. Blitz (editors), Techniques of Non-Destructive Testing (Butterworth & Co. (Publishers) Limited, 1960)

Table 1 Mechanical properties for materials used in the finite element modelling

	Young's modulus (GPa)	Shear modulus (GPa)	Poisson's ratio	Density (kg/m^3)
Lower wing skin (Aluminium)	$E = 71.00$	$G = 27.30$	$m = 0.33$	2700
Adhesive	$E = 2.17$	$G = 0.84$	$m = 0.35$	1000
Boron/epoxy	$E_{11} = 156.00$	$G_{12} = 19.0$	$m_{12} = 0.30$	2000
	$E_{22} = 30.00$	$G_{13} = 19.0$	$m_{13} = 0.30$	
	$E_{33} = 30.00$	$G_{23} = 11.5$	$m_{23} = 0.30$	

Table 2 Dimensions of notch with profiles shown in Figure 4

Notch	d_1 (mm)	d_2 (mm)	d_3 (mm)
No notch	-	-	-
33% notch	7.92	1.20	2.53
67% notch	16.08	2.40	5.15
100% through notch	24.00	3.60	7.68
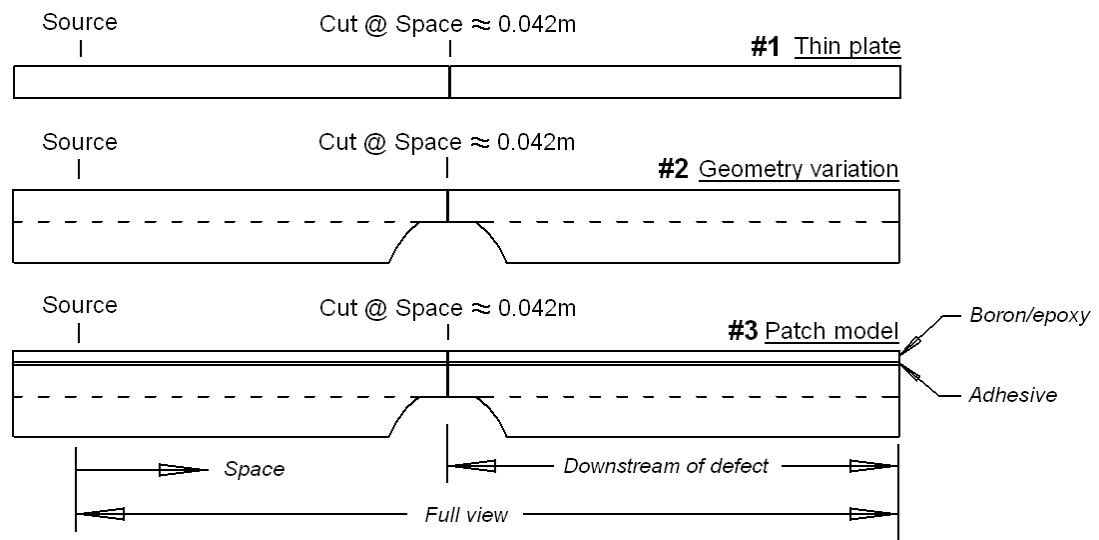
Figure 1 Schematic of three models used for finite element analysis
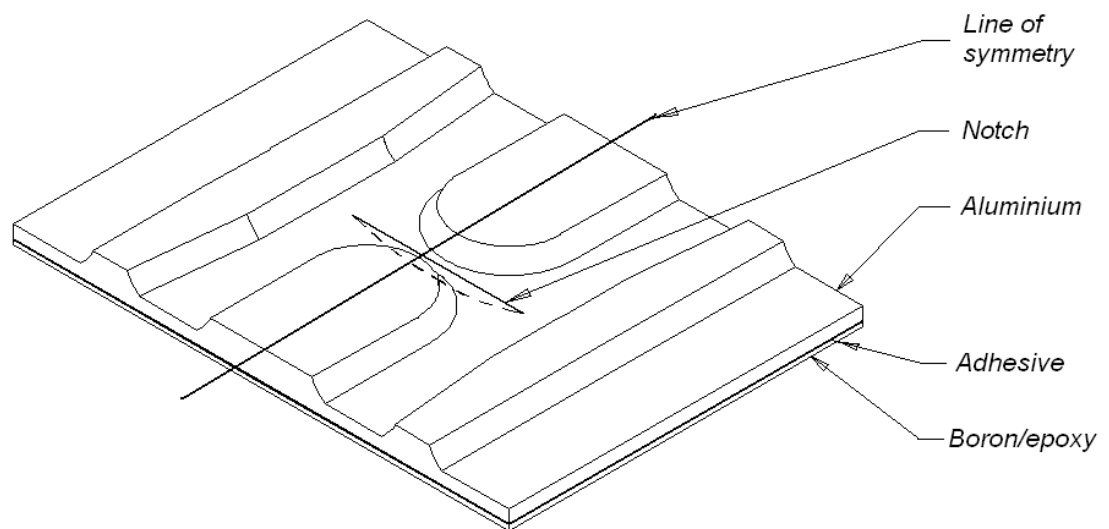
Figure 2 Schematic of F111 underwing skin
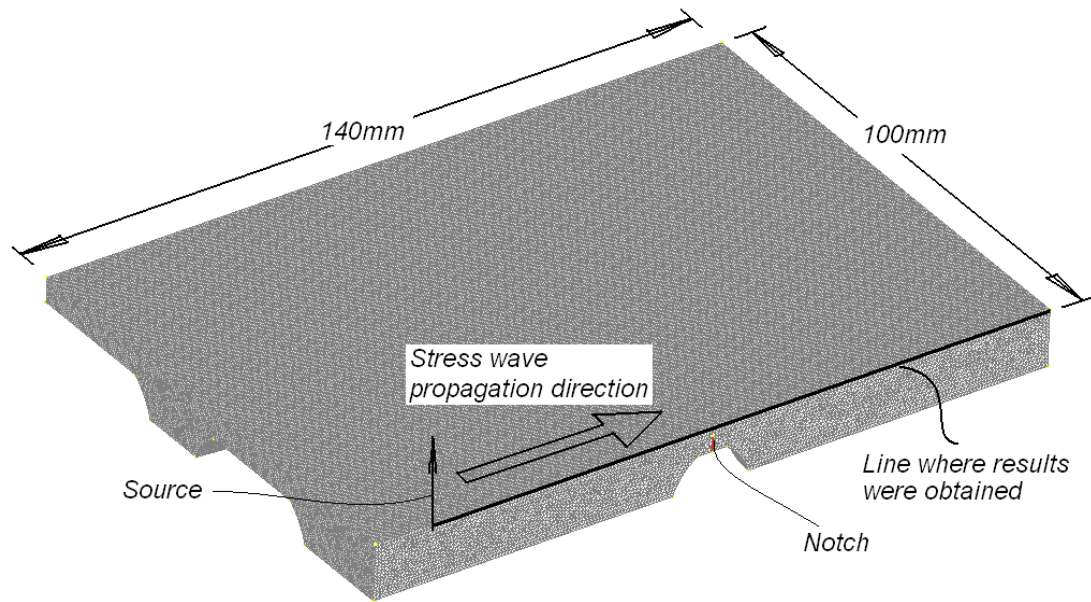
Figure 3 Finite element model of Figure 2
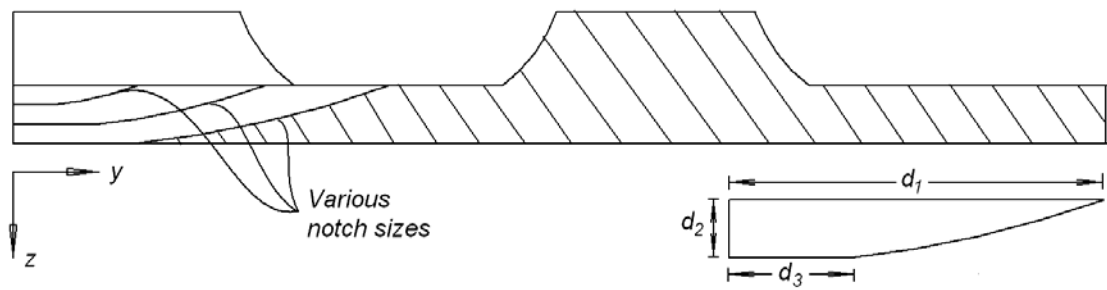
Figure 4 Profile of notches
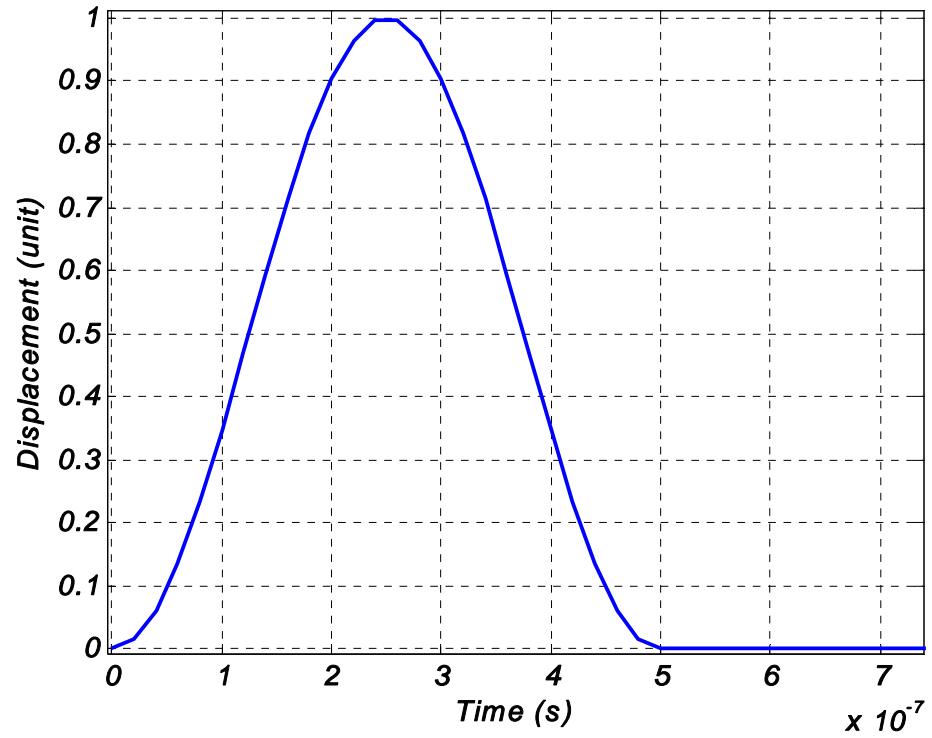
(a)
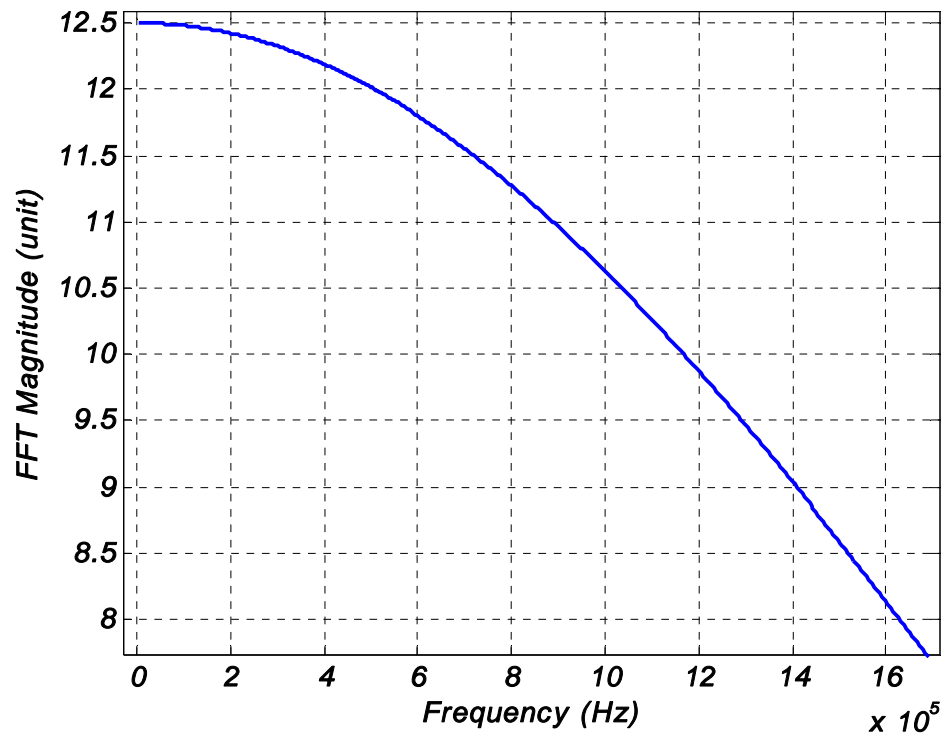
(b)

Figure 5 Excitation pulse (a) time domain (b) frequency domain
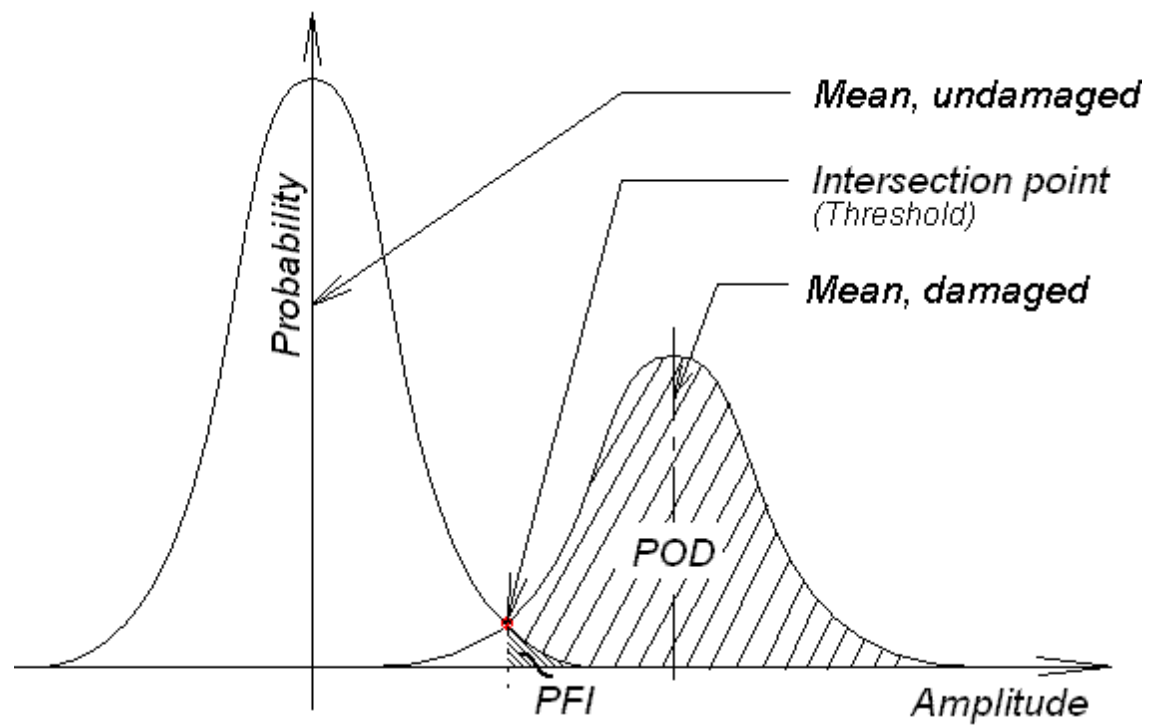
Figure 6 Sample probability distribution for undamaged- and damaged-case signals
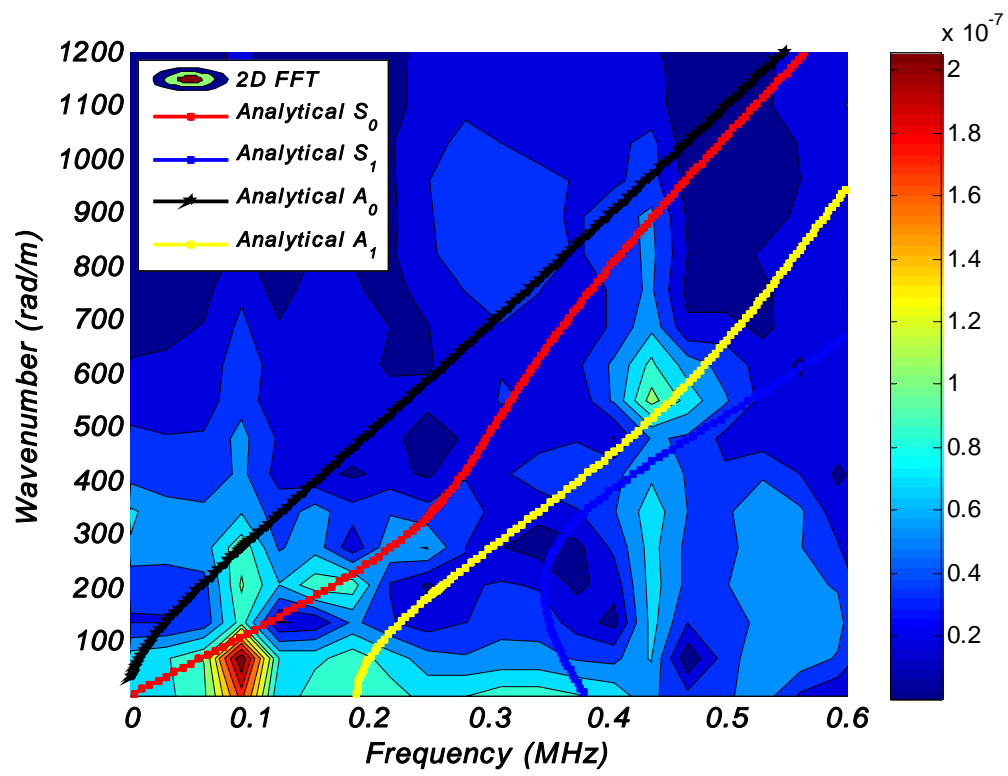
Figure 7 Two-dimensional fast Fourier transform (2D FFT) for an undamaged flat plate
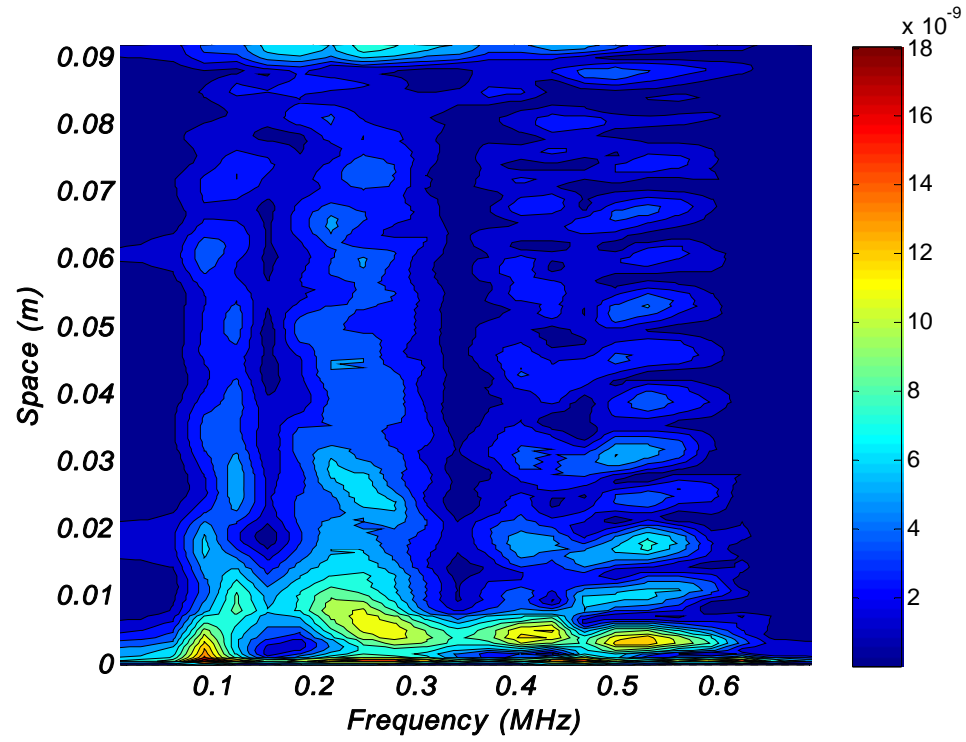
(a)
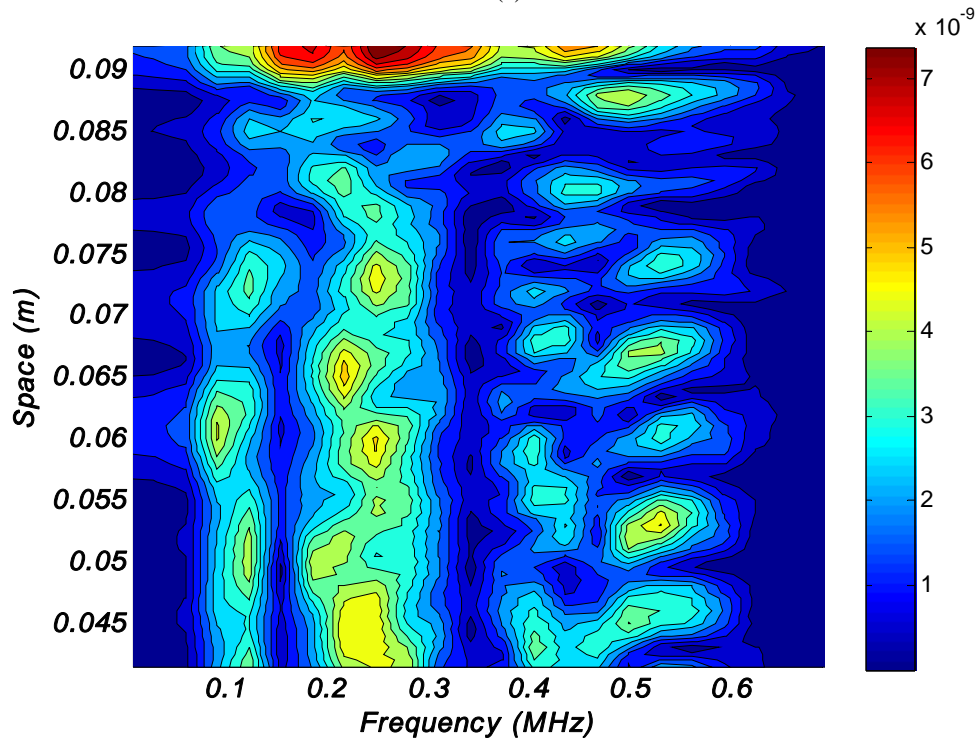
(b)

Figure 8 Temporal – spatial characteristics for an undamaged flat plate
(a) along the measurement line (b) region downstream of defect
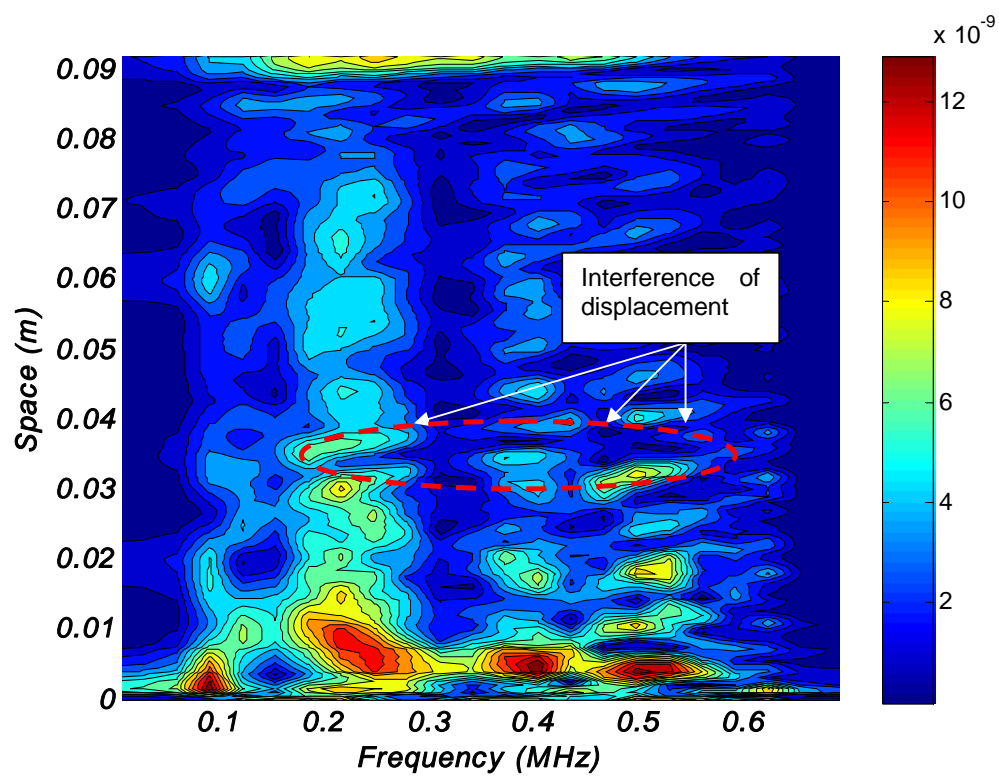
Figure 9 Temporal - spatial characteristics for 33% defect flat plate
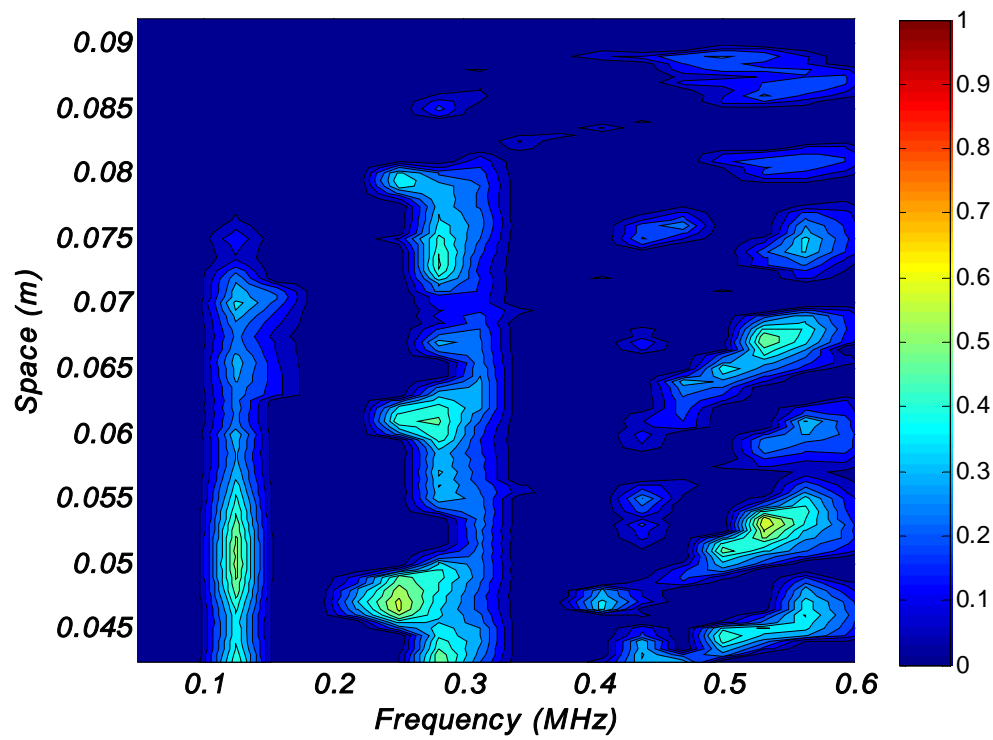
Figure 10 POD for 33% defect flat plate

Interference of stress waves
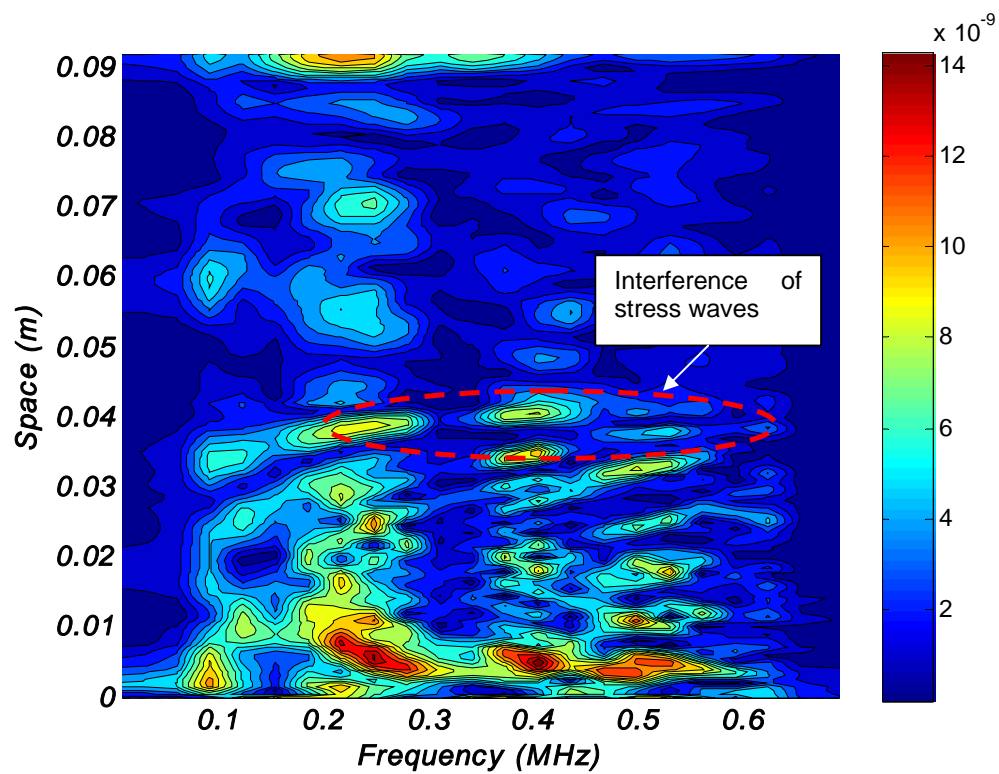
Figure 11 Temporal - spatial characteristics for 67% defect flat plate
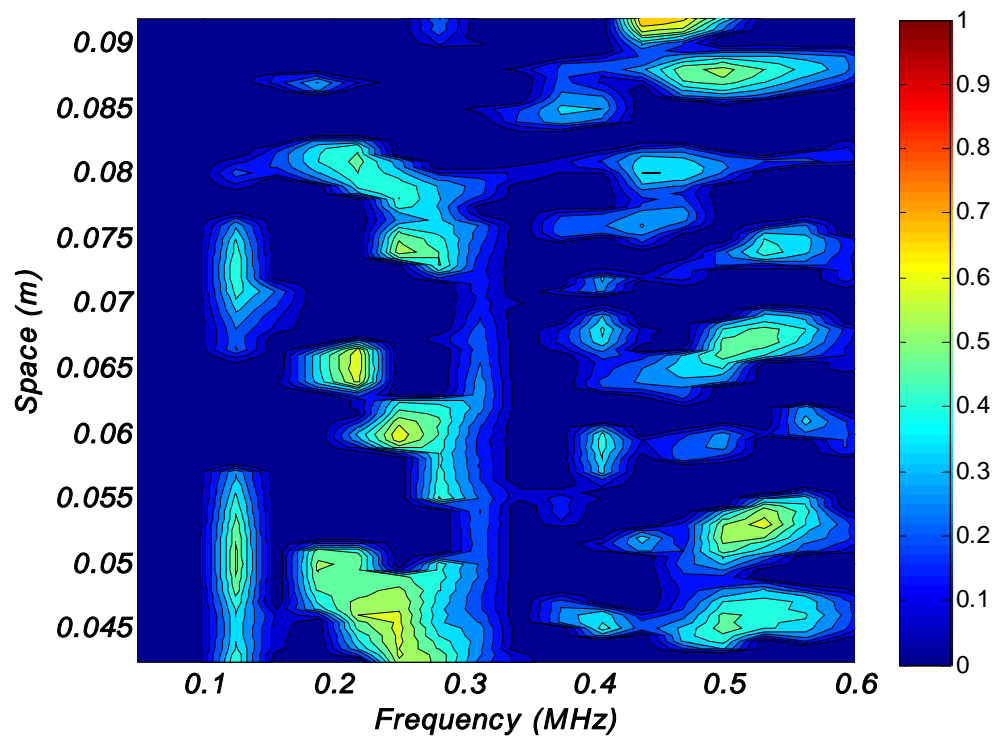
Figure 12 POD for 67% defect flat plate
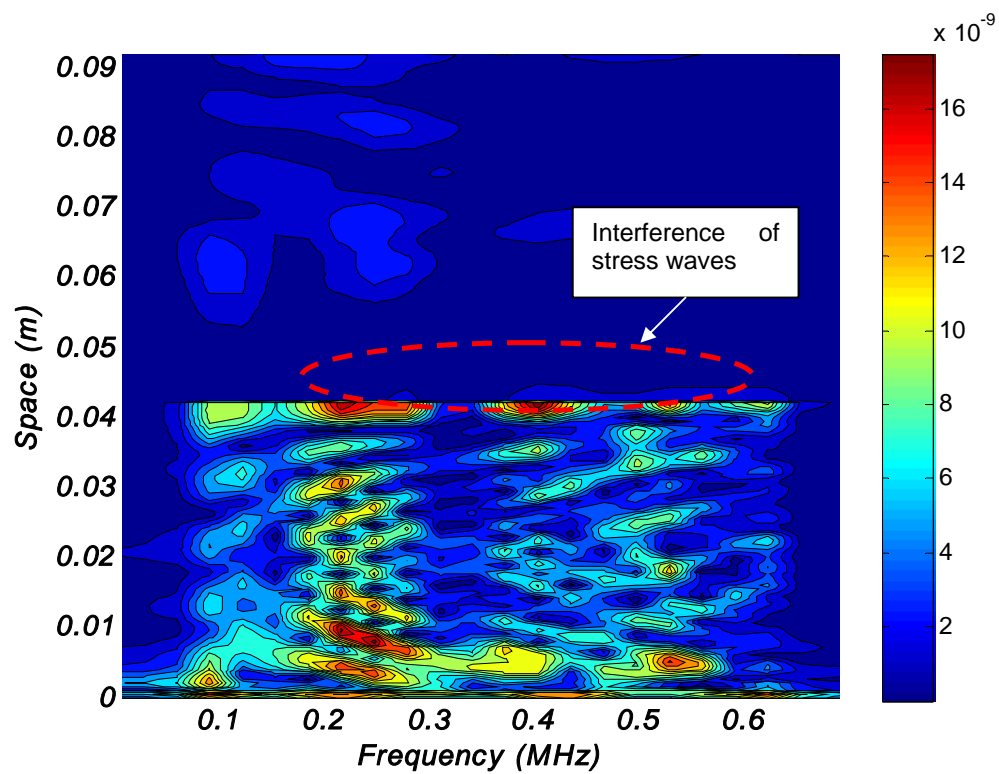
Figure 13 Temporal - spatial characteristics for surface penetrating defect, flat plate
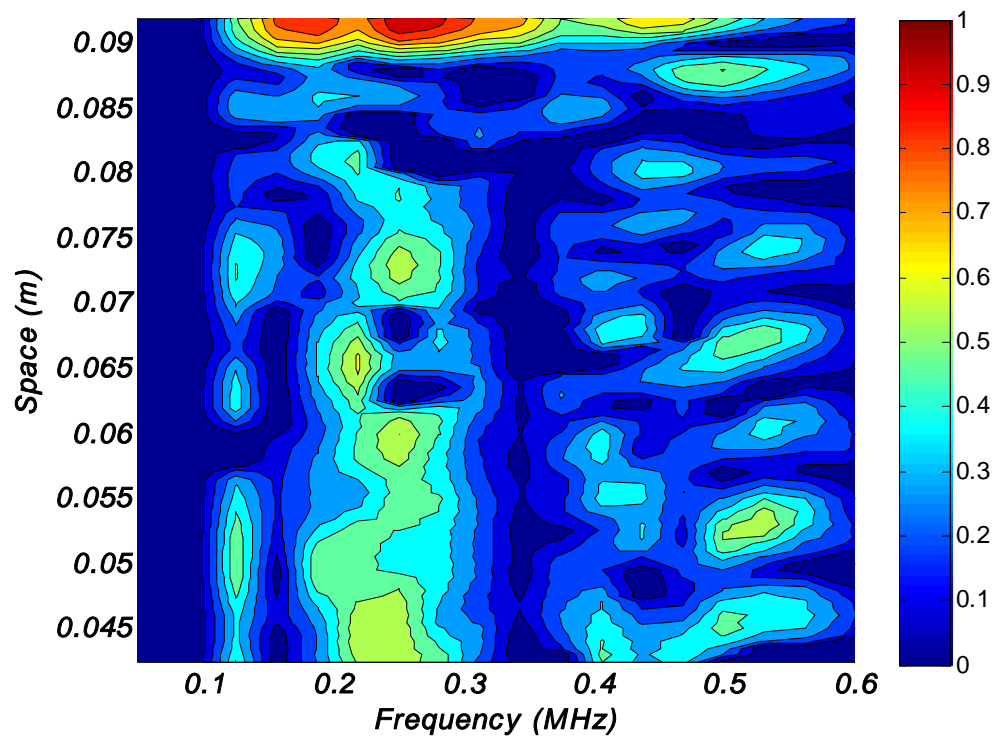
Figure 14 POD for surface-penetrating defect flat plate
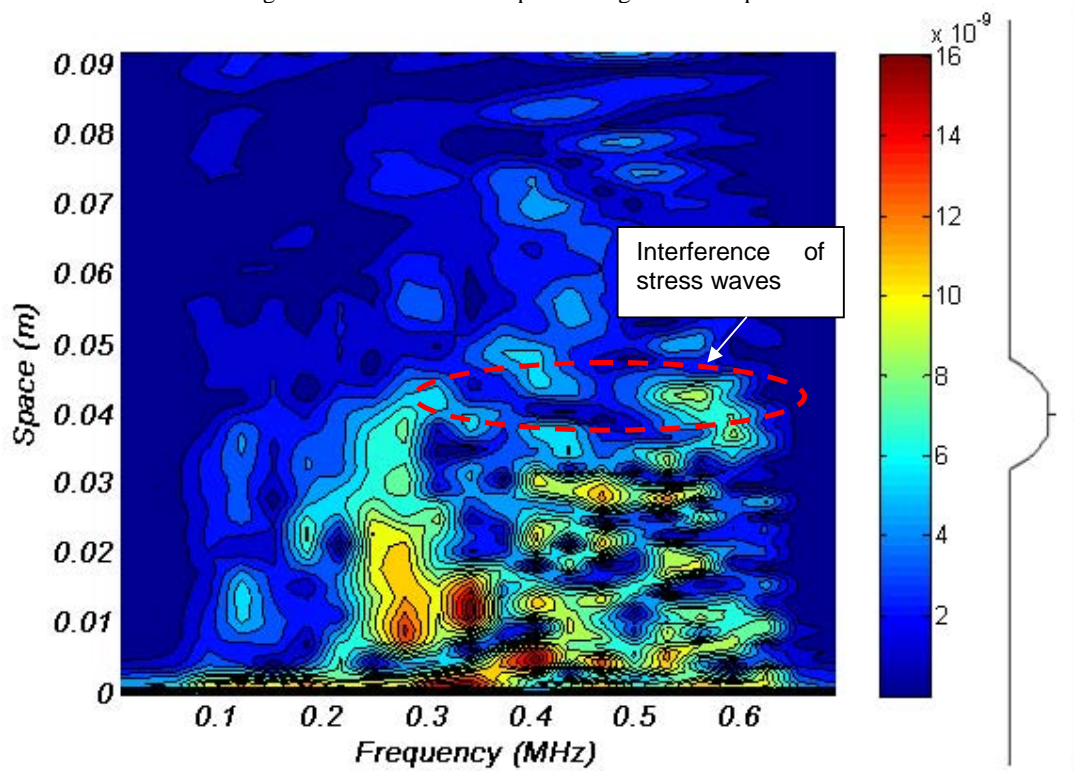
Figure 15 Temporal - spatial characteristics for no surface penetrating defect, geometry variation
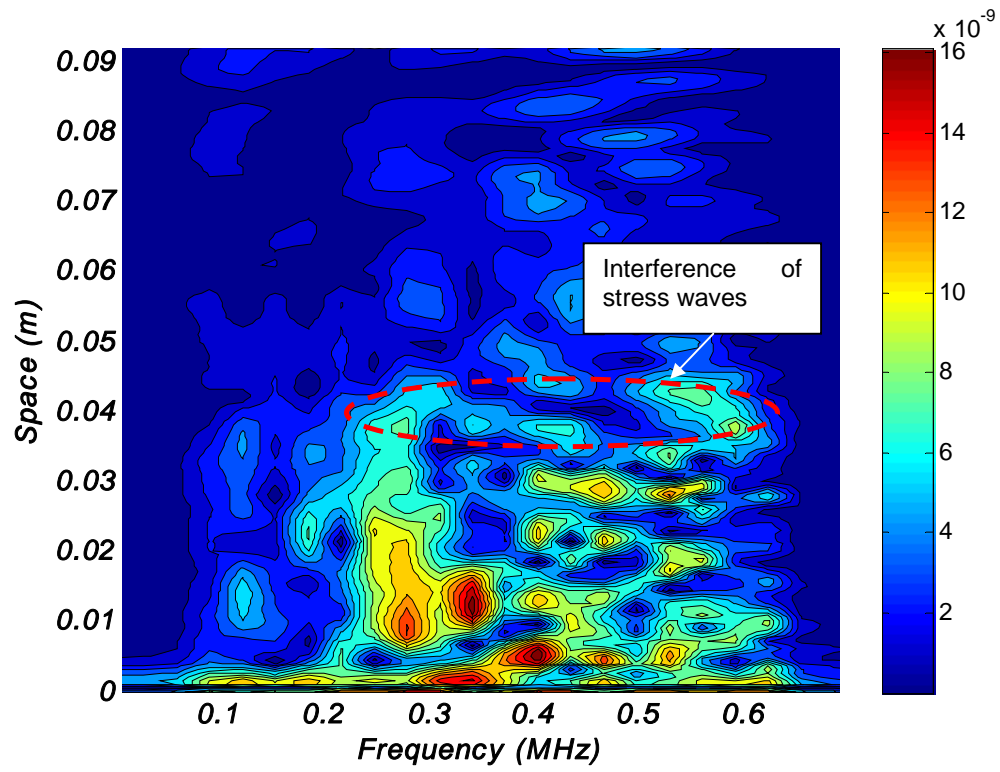
Figure 16 Temporal - spatial characteristics for 33% defect geometry variation case
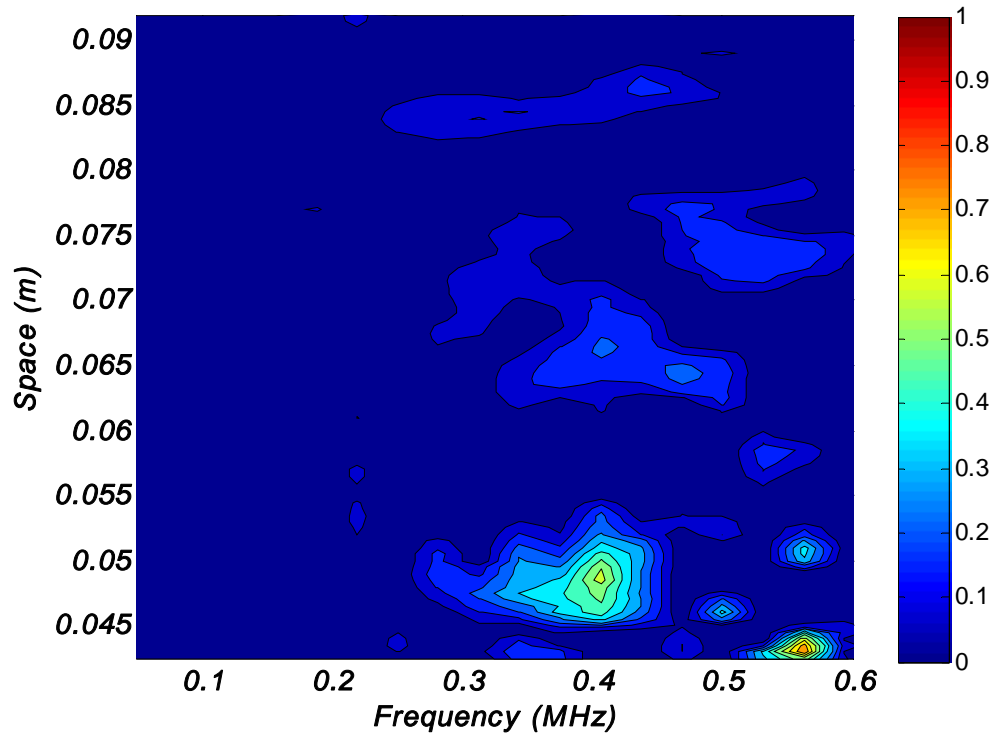
Figure 17 POD for 33% defect geometry variation case
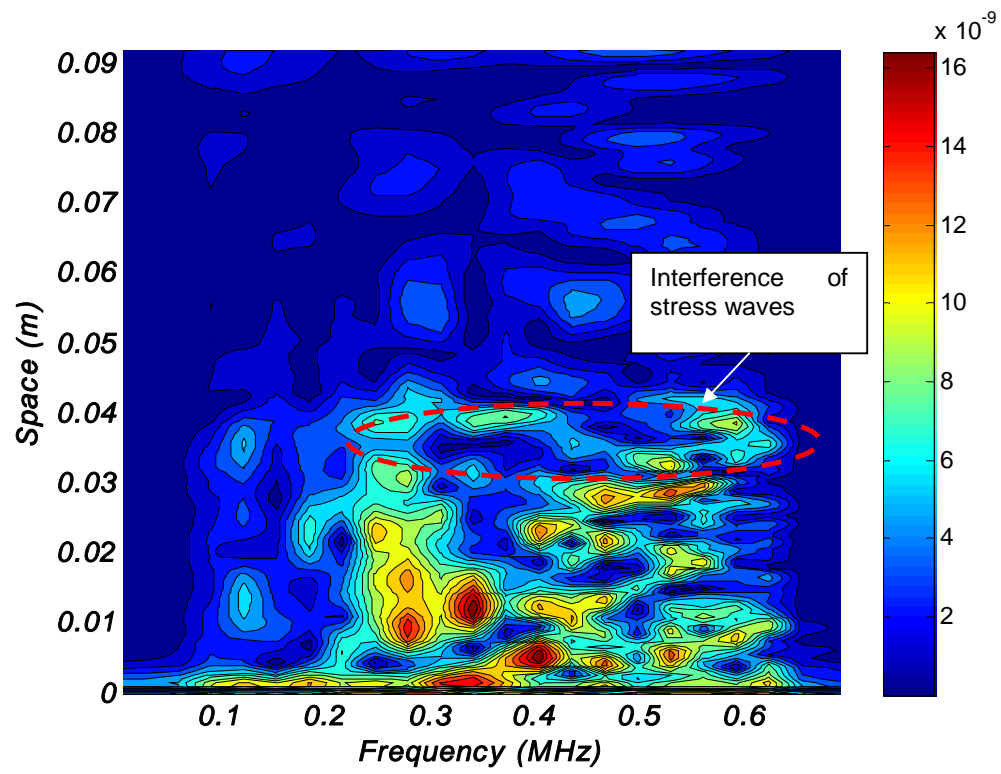
Figure 18 Temporal - spatial characteristics for 67% defect geometry variation case
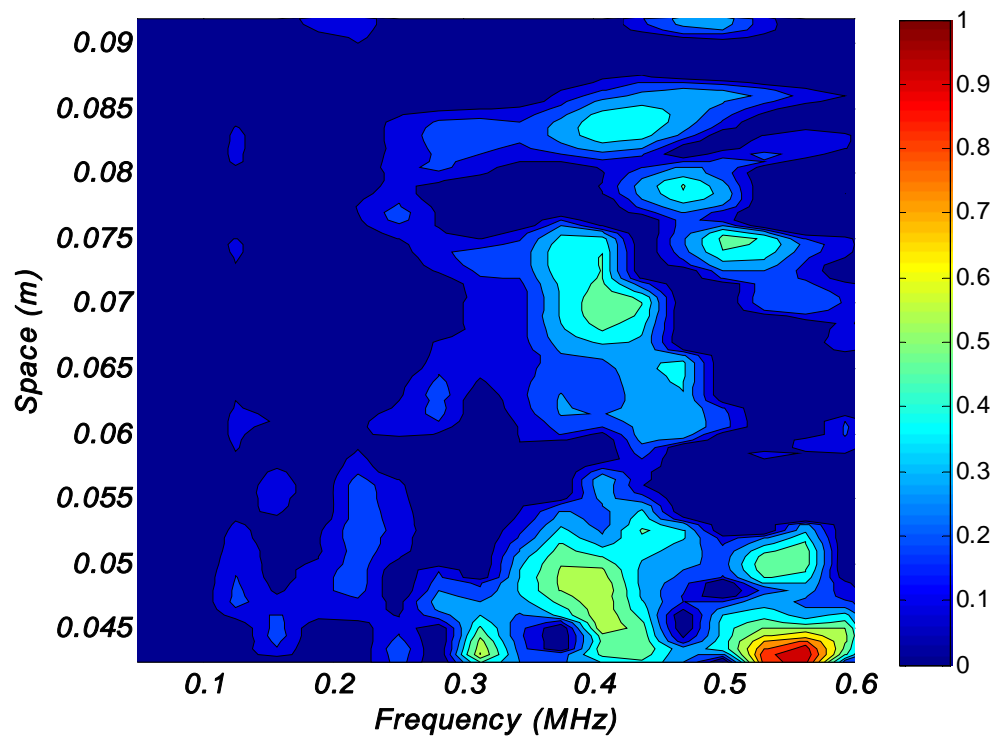
Figure 19 POD for 67% defect geometry variation case
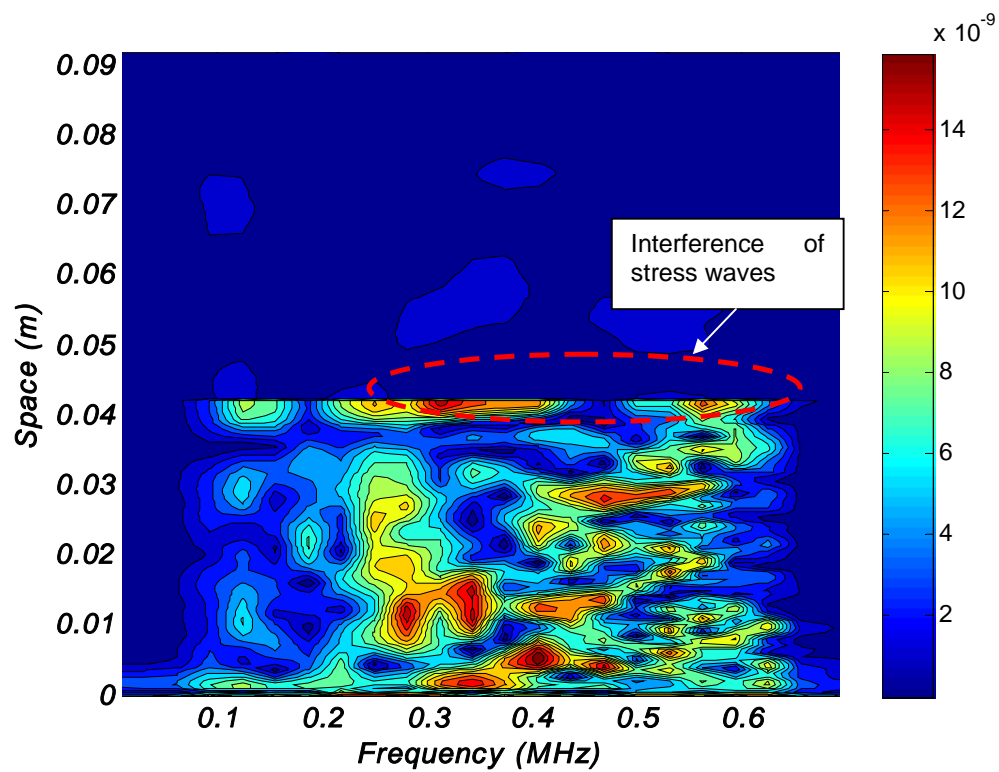
Figure 20 Temporal - spatial characteristics for surface-penetrating defect geometry variation case
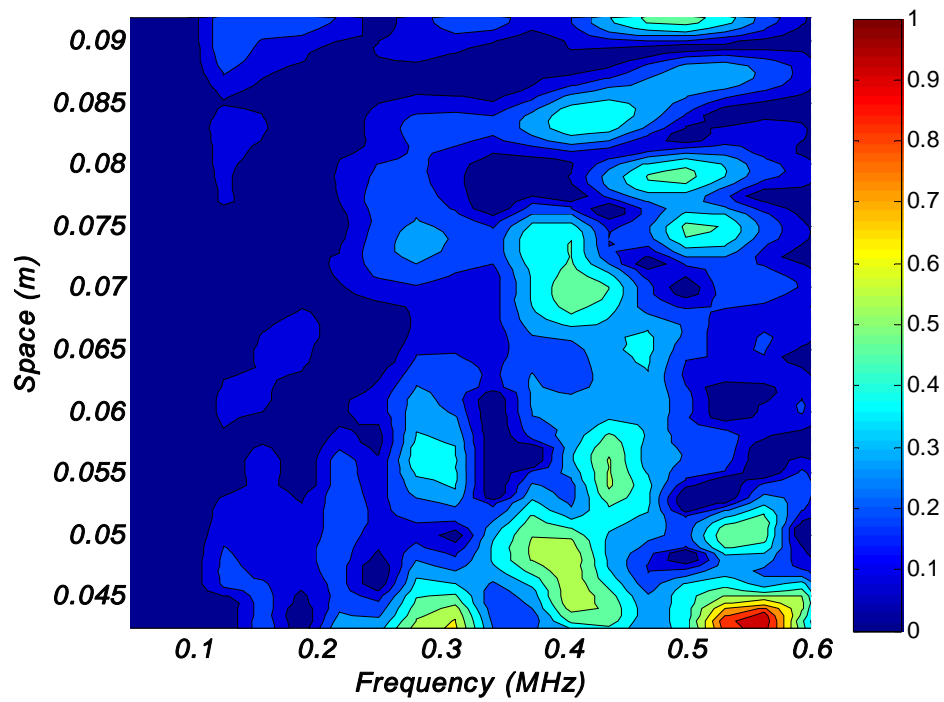
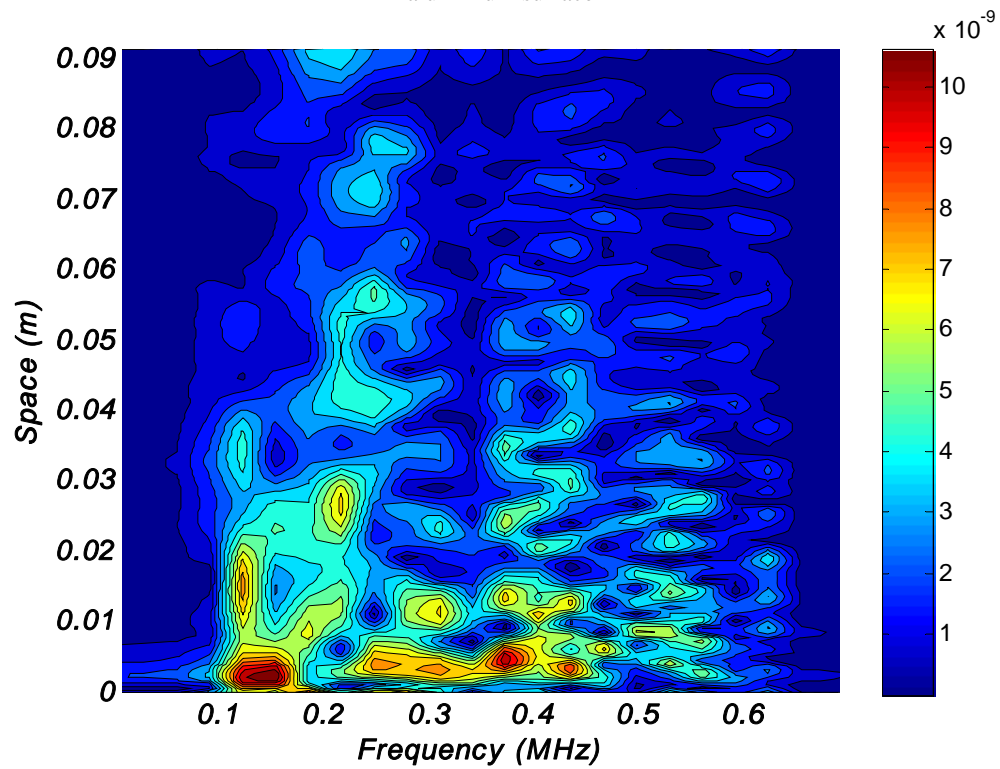Figure 21 POD for surface-penetrating defect geometry variation case
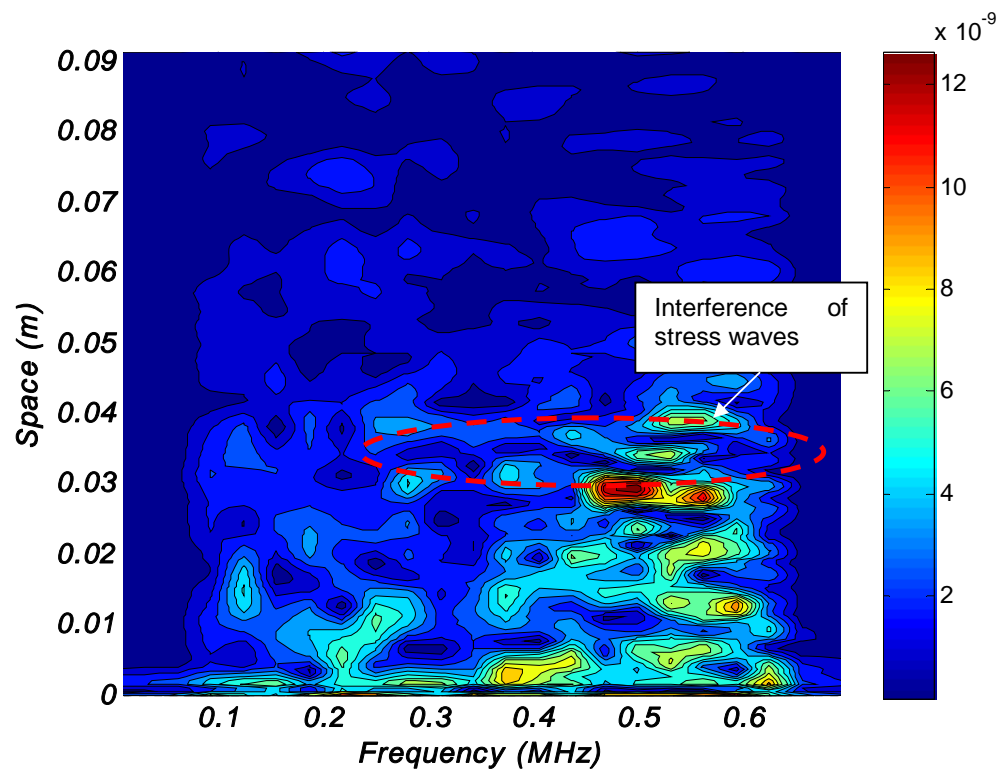
Figure 22 Temporal – spatial characteristics of stress wave for undamaged repaired structure on aluminium surface
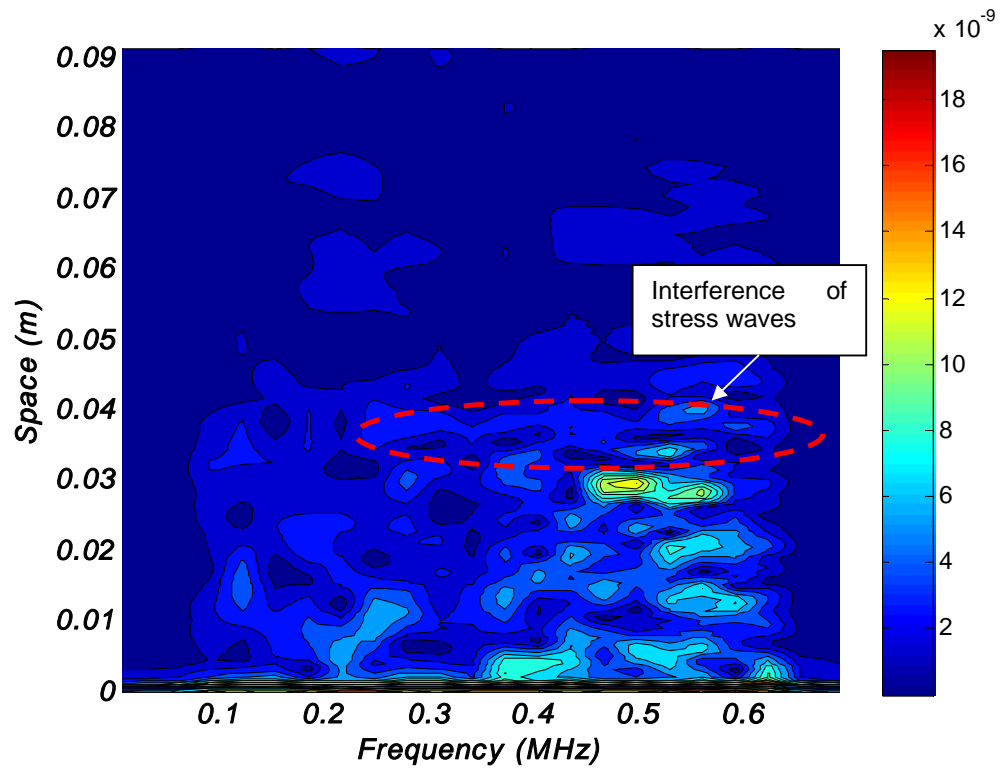
Figure 23 Temporal – spatial characteristics of stress wave for 33% defect repaired structure on aluminium surface
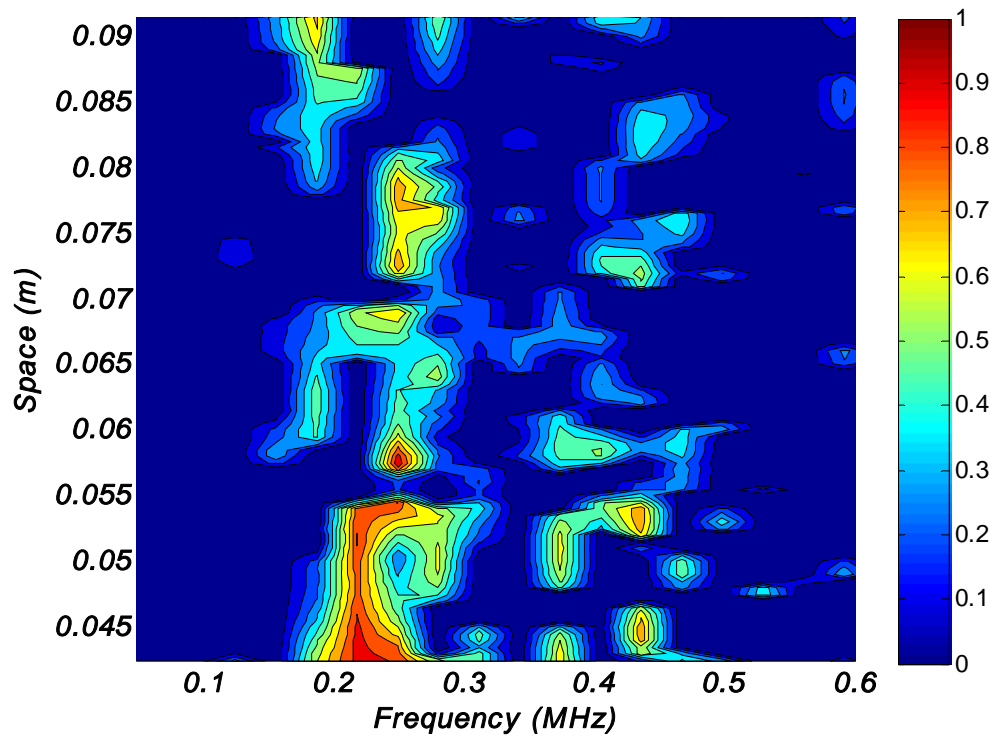
Figure 24 POD for 33% defect repaired structure on aluminium surface
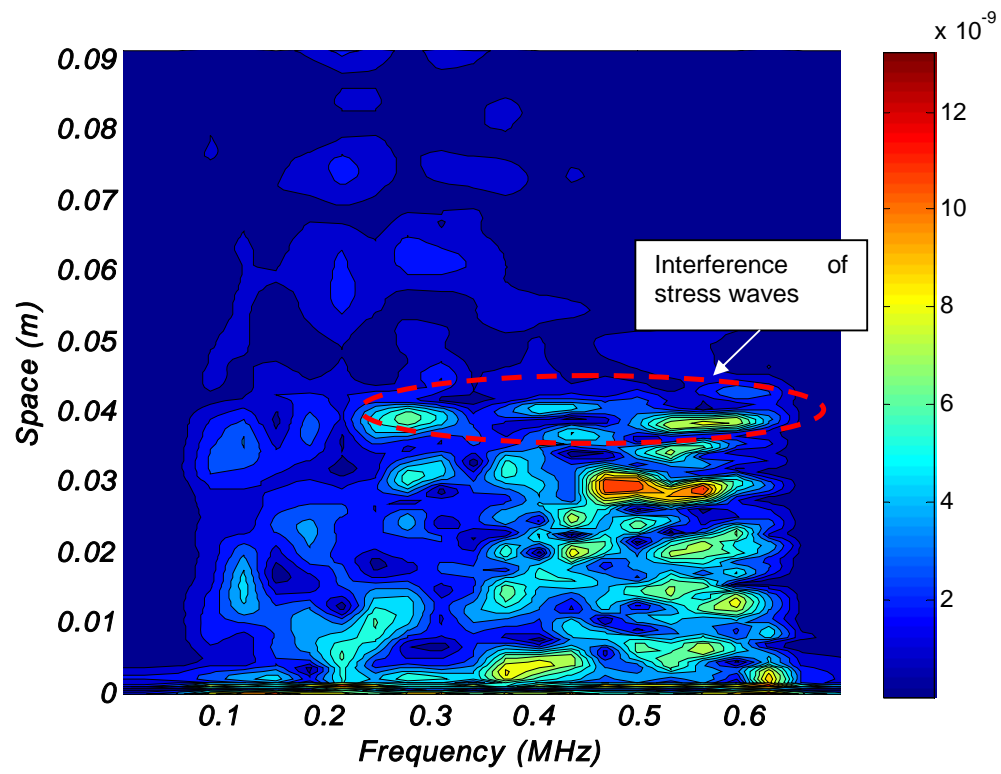
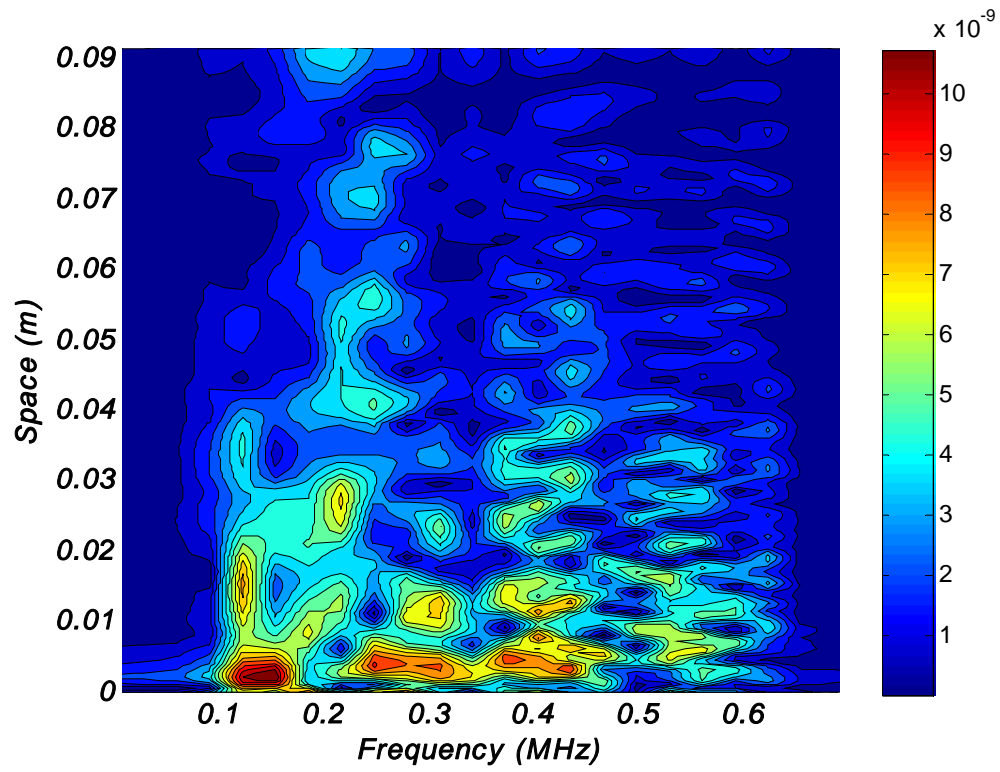Figure 25 Temporal – spatial characteristics of stress wave for 67% defect repaired structure on aluminium surface
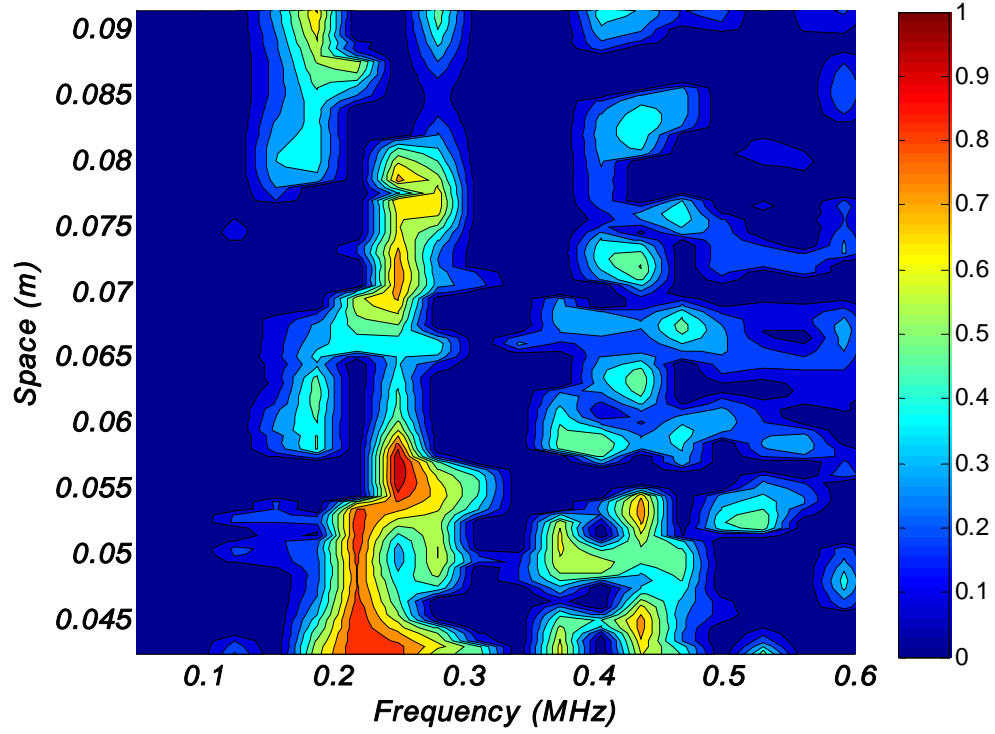
Figure 26 POD for 67% defect repaired structure on aluminium surface
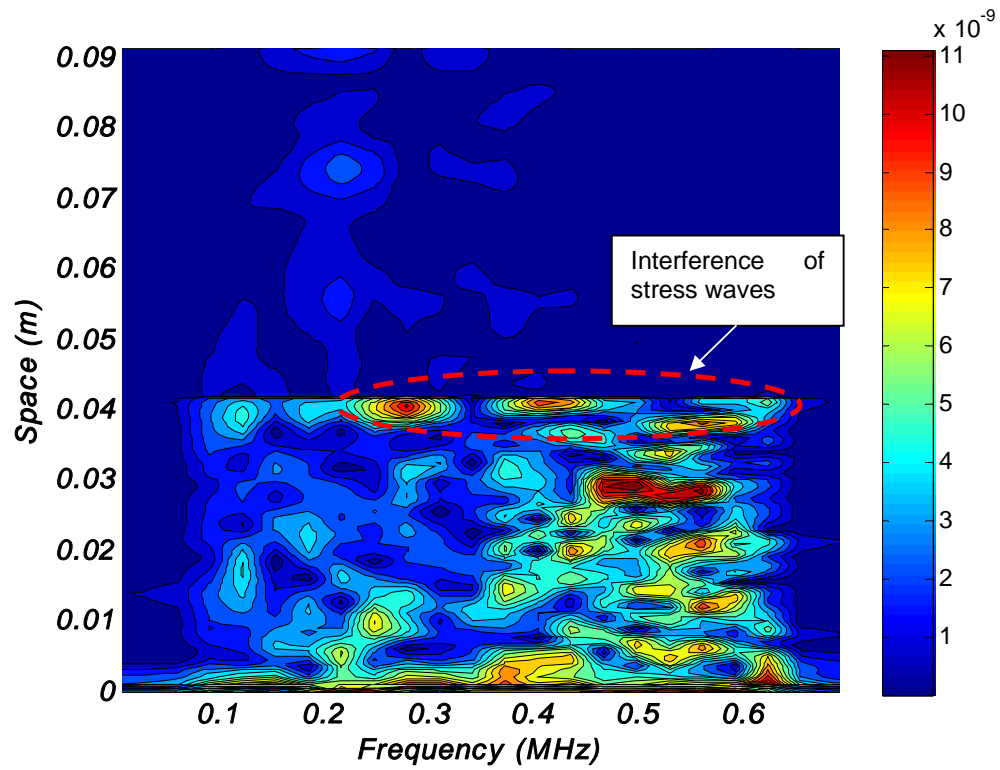
Figure 27 Temporal – spatial characteristics for surface-penetrating defect case, for repaired structure on aluminium surface
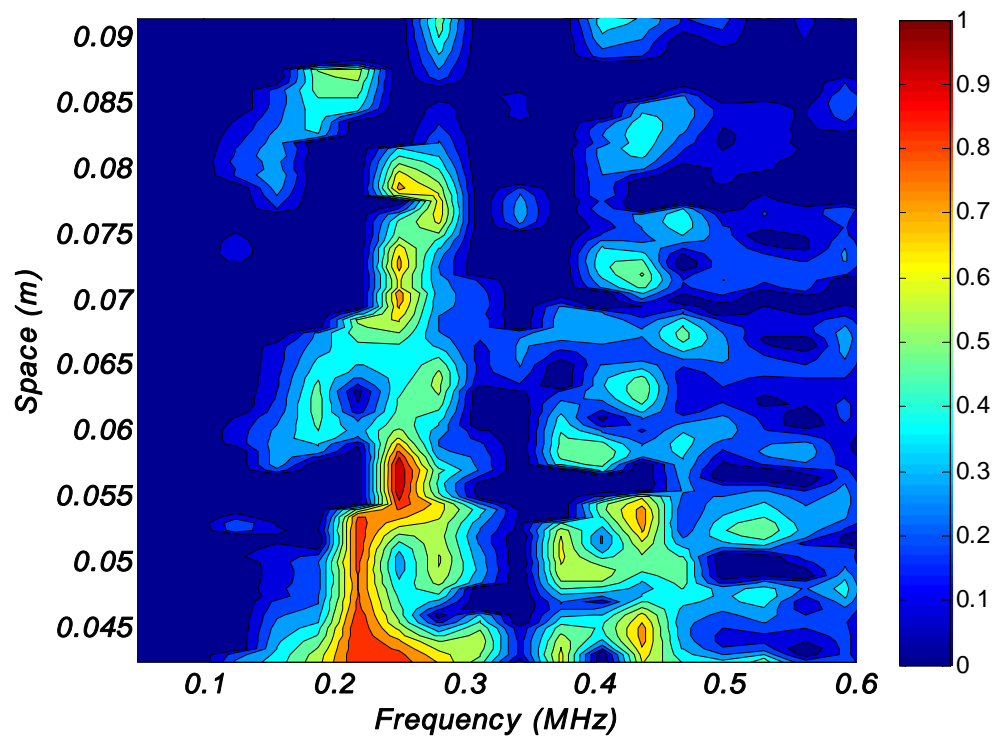
Figure 28 POD for surface-penetrating defect geometry variation case, for repaired structure on aluminium surface

Figure 29 Temporal – spatial characteristics of stress waves for repaired structure on boron/epoxy surface

Figure 30 Temporal – spatial characteristics for 33% defect repaired structure on boron/epoxy surface
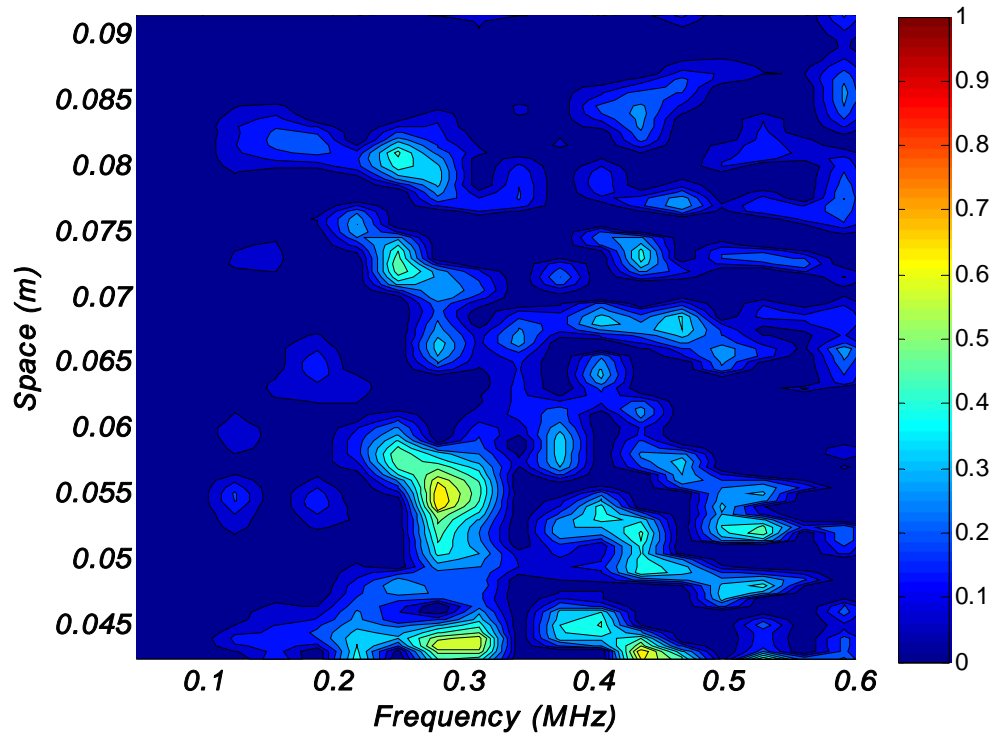
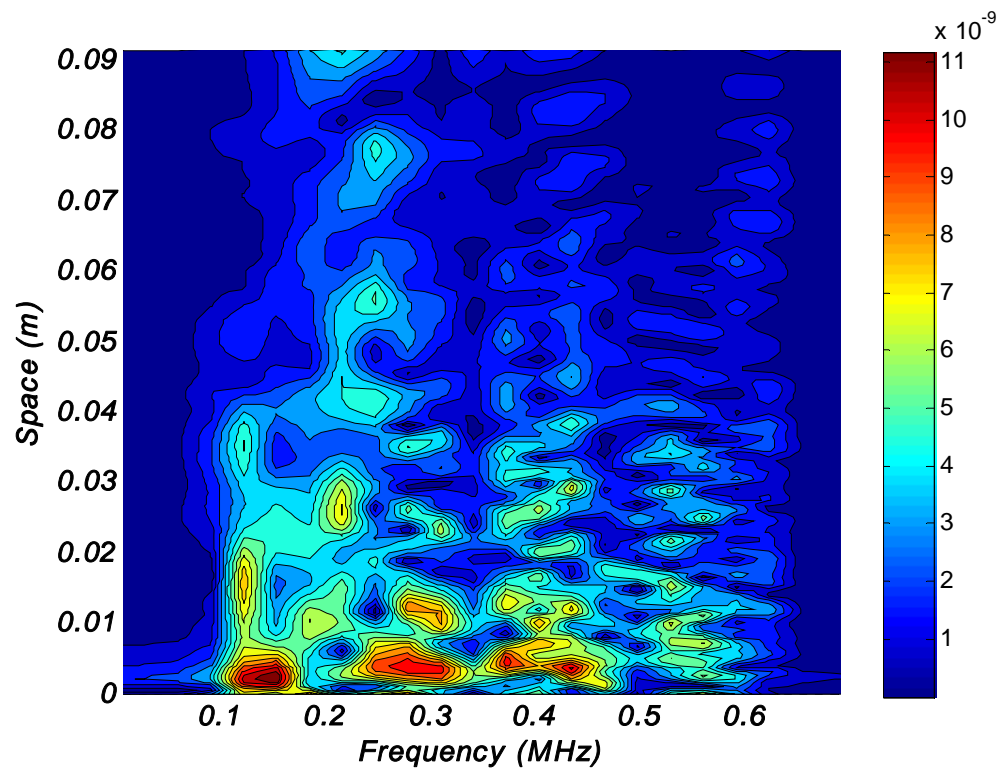Figure 31 POD for 33% defect repaired structure on boron/epoxy surface

Figure 32 Temporal – spatial characteristics for 67% defect repaired structure on boron/epoxy surface
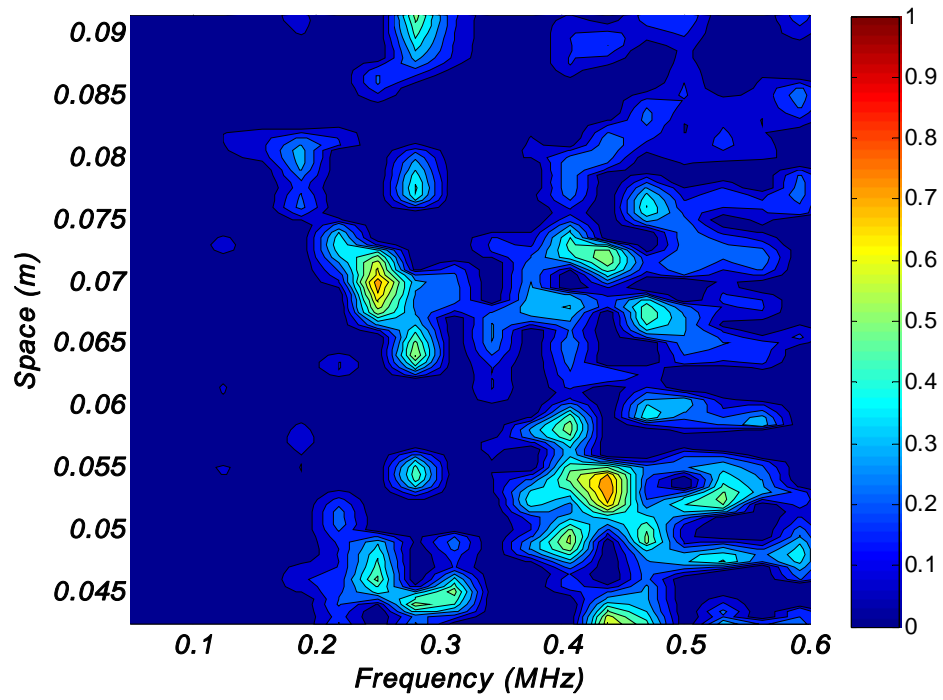
Figure 33 POD for 67% defect repaired structure on boron/epoxy surface
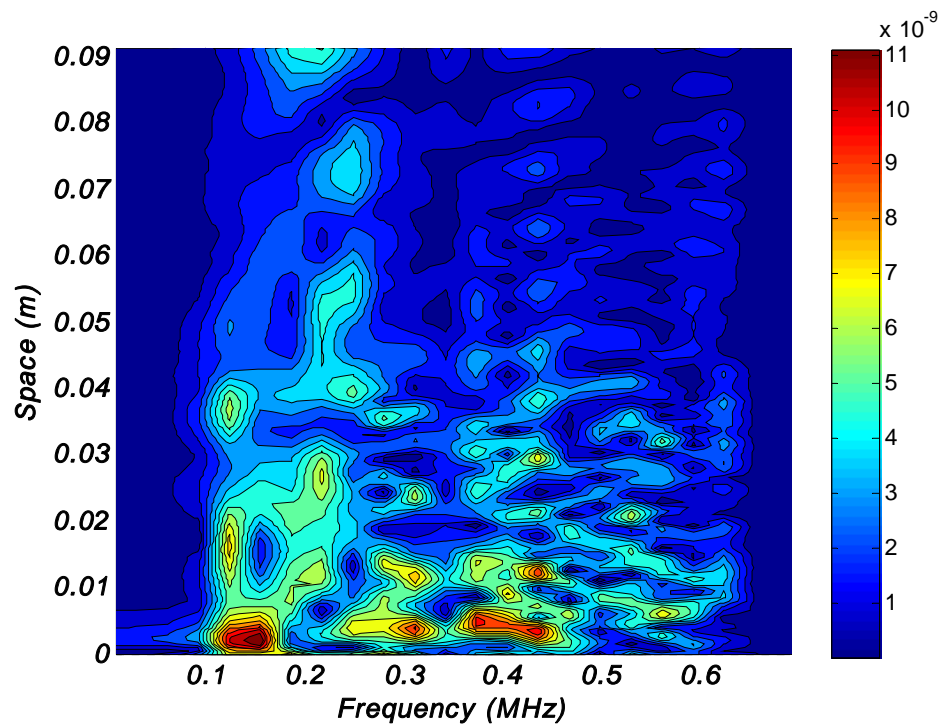

Figure 34 Temporal – spatial characteristics for surface-penetrating defect case, for repaired structure on boron/epoxy surface
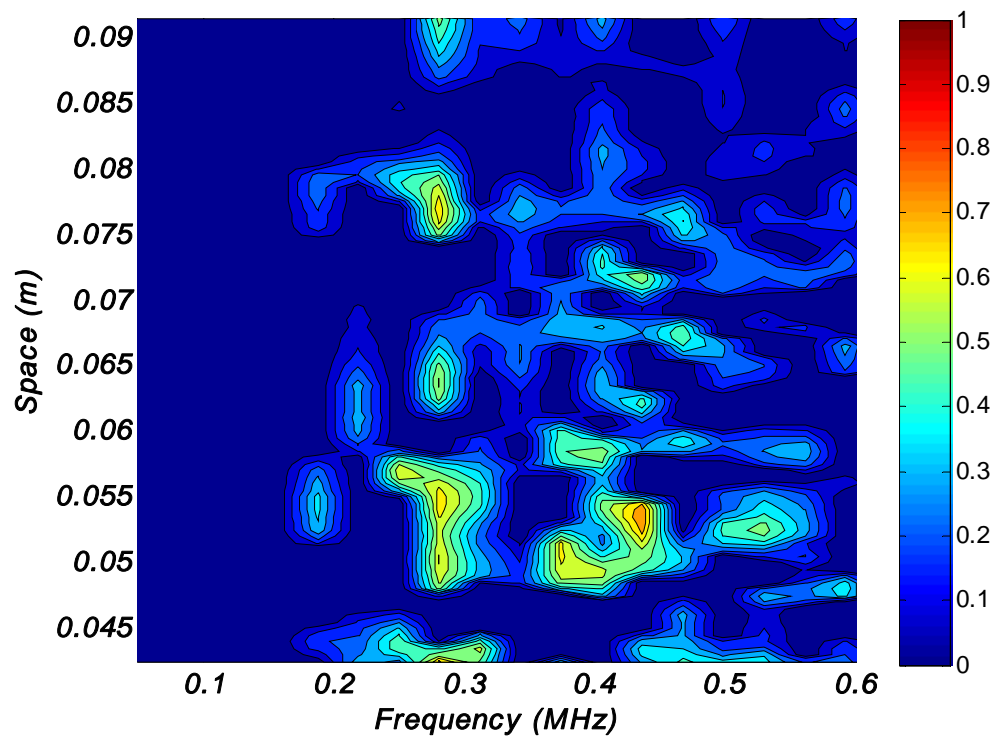
Figure 35 POD for surface-penetrating defect geometry variation case, for repaired structure on boron/epoxy surface